BRAF^{V600E} induces reversible mitotic arrest in human melanocytes via microRNA-mediated suppression of AURKB.

Andrew S. McNeal[1], Rachel L. Belote[2,*], Hanlin Zeng[2,*], Kendra Barker[2], Rodrigo Torres[1,3], Meghan Curtin[2], A. Hunter Shain[1,3], Robert H. I. Andtbacka[2,4], Sheri L. Holmen[2,4,5], David H. Lum[2], Timothy H. McCalmont[6], Matthew W. VanBrocklin[2,4,5], Douglas Grossman[2,5,,7], Maria L. Wei[1,3,8], Ursula E. Lang[1,3,6], and Robert L. Judson-Torres[2,5,7,†]

[1] Helen Diller Family Comprehensive Cancer Center, University of California San Francisco, San Francisco, CA, 94158, USA.
[2] Huntsman Cancer Institute, University of Utah, Salt Lake City, UT, 84112, USA.
[3] Department of Dermatology, University of California San Francisco, San Francisco, CA, 94115, USA.
[4] Department of Surgery, University of Utah, Salt Lake City, UT, 84132, USA.
[5] Department of Oncological Sciences, University of Utah, Salt Lake City, UT, 84132, USA.
[6] Department of Pathology, University of California San Francisco, San Francisco, CA, 94143, USA.
[7] Department of Dermatology, University of Utah, Salt Lake City, UT, 84102, USA.
[8] San Francisco Veterans Affairs Medical Center, San Francisco, San Francisco, CA, 94121, USA.

*These authors contributed equally
† To whom correspondence should be addressed. Tel: +1 801-213-8436; Email: judsontorreslab@gmail.com

Abstract

Benign melanocytic nevi frequently emerge when an acquired *BRAF^{V600E}* mutation triggers unchecked proliferation and subsequent arrest in melanocytes. Recent observations have challenged the role of oncogene-induced senescence in melanocytic nevus formation, necessitating investigations into alternative mechanisms for the establishment and maintenance of proliferation arrest in nevi. We compared the transcriptomes of melanocytes from healthy human skin, nevi, and melanomas arisen from nevi and identified a set of microRNAs as highly expressed nevus-enriched transcripts. Two of these microRNAs – MIR211-5p and MIR328-3p – induced mitotic failure, genome duplication and proliferation arrest in human melanocytes through convergent targeting of AURKB. We demonstrate that *BRAF^{V600E}* induces a similar proliferation arrest in primary human melanocytes that is both reversible and conditional. Specifically, *BRAF^{V600E}* expression stimulates either arrest or proliferation depending on the differentiation state of the melanocyte. We report genome duplication in human melanocytic nevi, reciprocal expression of AURKB and microRNAs in nevi and melanomas, and rescue of arrested human nevus cells with AURKB expression. Together, our data describe an alternative molecular mechanism for melanocytic nevus formation that is congruent with both experimental and clinical observations.

Introduction

Cutaneous melanoma is a potentially deadly skin cancer arising from the pigment-producing melanocytes of the human epidermis. An activating mutation in the BRAF proto-oncogene ($BRAF^{V600E}$) drives over half of all cutaneous melanomas[1–3]. Yet, when a melanocyte acquires a $BRAF^{V600E}$ mutation, the cell does not immediately transform to cancer. Instead, it usually undergoes clonal proliferation followed by stable arrest resulting in a benign skin lesion known as a melanocytic nevus or "mole"[3–6]. Despite the continued expression of $BRAF^{V600E}$, the majority of melanocytic nevi remain innocuous for the lifespan of the individual, suggesting that nevus cells have robust intrinsic defenses against hyperproliferation. By inducing hyperproliferation and subsequent arrest, the $BRAF^{V600E}$ mutation elicits divergent, biphasic phenotypes within a single cell – a poorly understood phenomenon. Characterization of the mechanisms and environmental factors that distinguish the two phenotypes could illuminate candidate strategies for chemoprevention of melanocytic nevus formation or interception of melanoma initiation.

The $BRAF^{V600E}$ mutation is clonally present in ~80% of human melanocytic nevi[3] and melanocyte-specific expression of the oncogene is sufficient to induce nevus formation in mice[6–8], suggesting that $BRAF^{V600E}$ drives proliferation arrest in melanocytes. The prevailing theory to explain this seemingly paradoxical role for $BRAF^{V600E}$ is oncogene-induced senescence (OIS)[9]. Cellular senescence is defined as the permanent cell-cycle arrest of previously replication-competent cells[10,11]. Senescence is associated with a variety of molecular hallmarks including elevated expression of $p16^{INK4A}$ and other cyclin-dependent-kinase inhibitors, TP53, H2AX, lysosomal beta-galactosidase and senescence-associated secretory proteins (SASP) as well as a DNA content profile indicative of arrest in the G0/G1 phases of the cell cycle[11–16]. The concept of OIS as a barrier to tumorigenesis derived from observations of a durable proliferation arrest induced by overexpression of oncogenic RAS or RAF in immortalized human fibroblasts[12,17].

More recent studies have questioned whether the term "senescence" aptly describes proliferation arrest of melanocytic nevi. Cell cycle re-entry that accompanies nevus recurrence[18], eruption[19], or transformation to primary melanoma suggests that the nevus arrest phenotype is reversible rather than permanent. Similarly, the expression of senescence markers do not readily distinguish human melanocytic nevi from primary or transformed melanocytes in humans (16^{INK4A}, TP53, H2AX and beta-galactosidase) or mice (any known hallmark of senescence)[8,20,21]. Setting aside the permanence of OIS, melanocytic nevus arrest was largely thought to be driven by induction of $p16^{INK4A}$ expression from the *CDKN2A* gene. Indeed, early studies demonstrated that $BRAF^{V600E}$ induces $p16^{INK4A}$ expression and that melanocytic nevi frequently express high levels of $p16^{INK4A}$ [9]. Despite this, $p16^{INK4A}$ expression is neither ubiquitous across melanocytic nevi, nor uniform within the cells of a single nevus[22,23], and neither knock down of the 16^{INK4A} transcript nor ablation of the *CDKN2A* locus prevents the onset or rescues $BRAF^{V600E}$-induced proliferation arrest[9,23–25]. $BRAF^{V600E}$ also stimulates expression of $p15^{INK4B}$ - the translational product of the *CDKN2B* gene[25] which is situated adjacent to the *CDKN2A* locus - suggesting $BRAF^{V600E}$

might orchestrate arrest via multiple cyclin dependent kinase inhibitors that induce arrest in the G1 phase of the cell cycle, prior to genome synthesis. While the loss of the *CDKN2A/B* locus is a formative event in melanoma progression, genetic evolution studies of melanoma progression suggest that selection against the *CDKN2A/B* locus occurs after BRAF^{V600E} melanocytes have already escaped nevus-associated arrest[23,26]. Collectively, these data complicate the straightforward model wherein BRAF^{V600E} induces the expression of cell cycle regulators leading to proliferation arrest, which is later circumvented by the genetic loss of those regulators.

Given these observations, we reasoned that the arrest response of human melanocytes to BRAF^{V600E} might be distinct from previous reports of BRAF^{V600E}-induced OIS in other cell types. Specifically, we hypothesized that nevus-associated arrest is conditional and coordinated by reversible changes in gene expression. Here, we identify a transcriptional program that is consistently elevated in melanocytic nevi and includes microRNAs (miRNAs) previously shown to have diagnostic value[27,28]. In parallel, we observe that, unlike RAF-induced OIS in fibroblasts, BRAF^{V600E}–induced arrest in human melanocytes is reversible and conditional. Merging these two observations, we discover that in melanocytes, regulation of miRNAs coupled to differentiation status permits toggling between BRAF^{V600E}-driven hyperproliferative to arrested phenotypes.

Results

Melanocytic nevus- enriched miRNAs induce mitotic failure and proliferation arrest in primary human melanocytes

Since melanocytic nevi do not consistently express known senescence markers, we sought to characterize the transcripts that are specifically elevated within nevus melanocytes (Fig. 1A). We analyzed previously published datasets comparing RNA expression between benign and malignant melanocytic lesions[26,28]. Each clinical specimen contained matched RNA samples derived from melanocytic nevi and melanomas that arose from those nevi. We reasoned that down-regulated transcripts within these newly-formed melanomas could represent the most immediate barriers to melanocyte growth. Of the differentially expressed genes (adjusted p value <0.05), six of the top ten with elevated expression in nevi were non-coding miRNAs (Fig. 1B and Table S1). Among these were miRNAs we and others have previously shown to be enriched in nevi compared to melanomas, including MIR211-5p, MIR125A-5p, MIR125B-5p and MIR328-3p[28,29]. To determine whether elevated expression of these miRNAs distinguished nevus melanocytes from normal epidermal melanocytes, we profiled melanocytes from fresh healthy skin and nevi (Table S2). Three of the miRNAs (MIR211-5p, MIR328-3p, MIR125B-5p) were also more highly expressed in melanocytic nevi as compared to healthy melanocytes or melanomas - an expression pattern consistent with enrichment in arrested melanocytes - whereas one miRNA (MIR125A-5p) presented a pattern consistent with lineage specific expression that is lost upon

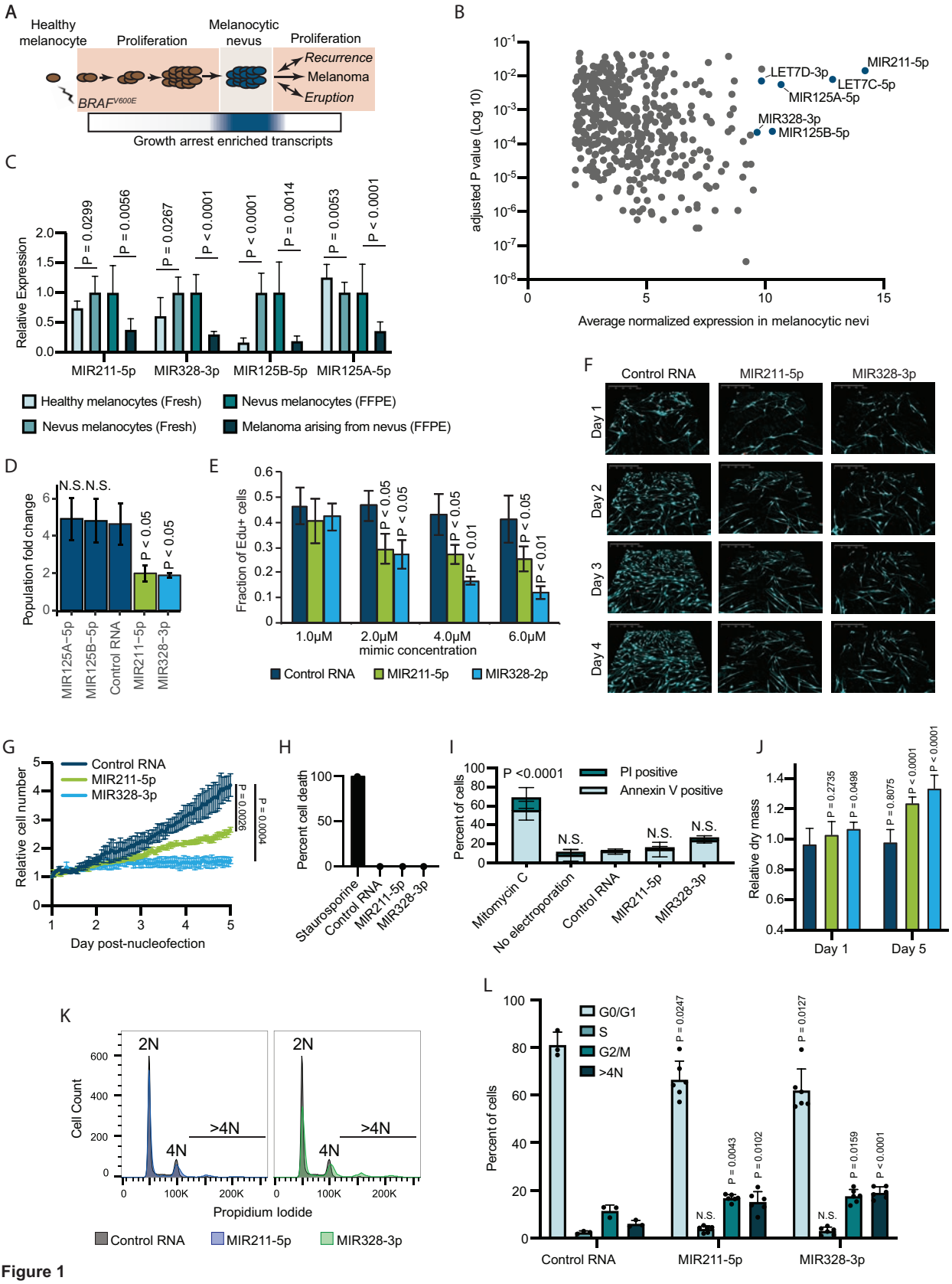
A
Healthy melanocyte
Proliferation
Melanocytic nevus
Proliferation
Recurrence
Melanoma
Eruption
BRAF V600E
Growth arrest enriched transcripts
B
adjusted P value (Log 10)
Average normalized expression in melanocytic nevi
LET7D-3p
MIR211-5p
LET7C-5p
MIR125A-5p
MIR328-3p
MIR125B-5p
C
Relative Expression
P = 0.0299
P = 0.0056
P = 0.0267
P < 0.0001
P < 0.0001
P = 0.0014
P = 0.0053
P < 0.0001
MIR211-5p
MIR328-3p
MIR125B-5p
MIR125A-5p
Healthy melanocytes (Fresh)
Nevus melanocytes (FFPE)
Nevus melanocytes (Fresh)
Melanoma arising from nevus (FFPE)
D
Population fold change
N.S.N.S.
P < 0.05
P < 0.05
MIR125A-5p
MIR125B-5p
Control RNA
MIR211-5p
MIR328-3p
E
Fraction of Edu+ cells
1.0μM
2.0μM
4.0μM
6.0μM
mimic concentration
Control RNA
MIR211-5p
MIR328-2p
F
Control RNA
MIR211-5p
MIR328-3p
Day 1
Day 2
Day 3
Day 4
G
Relative cell number
Control RNA
MIR211-5p
MIR328-3p
P = 0.0026
P = 0.0004
Day post-nucleofection
H
Percent cell death
Staurosporine
Control RNA
MIR211-5p
MIR328-3p
I
Percent of cells
P <0.0001
PI positive
Annexin V positive
N.S.
N.S.
N.S.
Mitomycin C
No electroporation
Control RNA
MIR211-5p
MIR328-3p
J
Relative dry mass
P = 0.2735
P = 0.0498
P = 0.8075
P < 0.0001
P < 0.0001
Day 1
Day 5
K
Cell Count
2N
4N
>4N
Propidium Iodide
Control RNA
MIR211-5p
MIR328-3p
L
Percent of cells
G0/G1
S
G2/M
>4N
P = 0.0247
P = 0.0043
P = 0.0102
P = 0.0127
P = 0.0159
P < 0.0001
N.S.
N.S.
Control RNA
MIR211-5p
MIR328-3p

Figure 1

113

Figure 1: Melanocytic nevus enriched miRNAs induce arrest in primary human melanocytes

(A) Schematic of hypothesized plastic nature of $BRAF^{V600E}$- and nevus- associated proliferation arrest. Expression of the predicted nevus enriched transcriptional program is highlighted in blue. **(B)** Scatter plot depicting gene expression combining publicly available sequencing datasets totaling 14 melanoma-arising-from-nevus specimens, dissected into benign and malignant portions (28 total samples). Plotted are the adjusted p values (DESeq2) comparing matched nevus and melanoma samples against average normalized expression in nevus portion. Only genes exhibiting both high expression and significant differential expression in nevus portions are plotted (see Methods). The full list of genes is included as Table S1. **(C)** Left two columns, the relative expression of indicated miRNAs in freshly isolated human melanocytes from $BRAF^{V600E}$ melanocytic nevi (n = 6) compared to $BRAF^{WT}$ healthy skin melanocytes (n = 8). Right two columns, the relative expression of indicated miRNAs in melanocytes dissected from FFPE nevus (n = 7) or melanoma (n = 7) specimens. Data represent mean and standard deviation of normalized RNA sequencing read counts relative to nevus-derived samples. **(D)** Mean and standard deviation for population fold change over seven days of melanocytes nucleofected with indicated miRNA mimics compared to non-targeting control (Control RNA) (n = 3). **(E)** Mean and standard deviation for fraction of EdU positive cells 4 days after nucleofection with indicated concentrations of miRNA mimics (n= 3). P values indicate comparisons to concentration matched control. **(F)** Representative QPI images of melanocytes nucleofected with indicated miRNA mimics. Pixel color indicates low (black), mid (blue) or high (red) optical density. **(G)** Mean and standard deviation for relative QPI-derived cell number over time (n = 3). **(H)** Mean and standard deviation for QPI-derived cell death counts as percentage of total cells imaged on day 1 (n = 3). Cells treated with 0.1 μM staurosporine were included as a control (n = 1) for induction of cell death. **(I)** Mean and standard deviation for percent Annexin V/PI positive cells nucleofected with indicated miRNA mimics (n = 3). Cells treated with 5μg/ml mitomycin C were included as a control (n = 3) for induction of apoptosis. **(J)** Mean and standard deviation for relative QPI-derived dry mass per cell (n = 3). Colors as in (E). **(K)** Representative histograms of DNA content profiling via propidium iodide incorporation measured by flow cytometry 5 days post- nucleofection of miRNA mimics. **(L)** Mean and standard deviation for percent of cells in indicated phases of cell cycle based upon profiles as in (K) (n = 3-6, individual datapoints shown). P values for D-L calculated by unpaired t tests comparing experimental to Control RNA. N.S. = not significant ($P \geq 0.05$)

transformation (Fig. 1C). We conclude that MIR211-5p, MIR328-3p, MIR125B-5p are transcripts specifically enriched in arrested melanocytic nevi.

To investigate whether elevated expression of MIR211-5p, MIR328-3p, or MIR125B-5p induce melanocytic arrest, we introduced synthesized mimetics of the mature miRNAs into primary human melanocytes and tracked proliferation over seven days in culture. The introduction of either MIR211-5p or MIR328-3p resulted in significantly fewer melanocytes compared to a non-targeting control (Fig. 1D). Increased concentrations of these mimics resulted in a dose-dependent decrease in EdU uptake, consistent with a cell cycle defect (Fig. 1E). To better characterize the effect of MIR211-5p or MIR328-3p expression on cell cycle and cell viability, we performed time-lapsed quantitative phase imaging (QPI). We and others have previously established QPI as a method for adherent cell cytometry that can simultaneously measure melanocyte proliferation, cell death, and cell cycle stage with single cell resolution[30–32]. Images were taken every hour for 5 days post-nucleofection (Fig. 1F). Cells expressing MIR211-5p or MIR328-3p exhibited significantly reduced growth curves (Fig. 1G). We observed no evidence of increased cell death (Fig. 1H), and confirmed this result with Annexin V staining (Fig. 1I). Thus, MIR211-5p and MIR328-3p induce proliferation arrest in human melanocytes.

156
157 Further characterization of the QPI images revealed a distinct increase in intra-cellular dry mass in
158 proliferation-arrested conditions (Fig. 1J). The dry mass of a cell is a measurement of total biomass (DNA,
159 RNA, proteins, lipids, etc) and is quantitatively measured by QPI. Relative dry mass fluctuates with cell
160 cycle stage in a predictable manner[30]. The 20-40% increase we observed here is characteristic of cells
161 that have doubled their DNA content but failed to complete mitosis. We confirmed this finding by
162 measuring DNA content of the arrested populations (Fig. 1K). We observed significant increases of cells
163 with both 4N DNA content and greater than 4N DNA content, indicative of cytokinetic failure following
164 DNA replication. Consistent with this interpretation, time-lapsed imaging revealed incidences of tripolar
165 mitosis and anaphase bridging in miRNA-expression melanocytes – both processes associated with
166 cytokinetic failure[33] - which were not observed in control conditions or standard culture (Supplemental
167 Files 1 and 2). We conclude that MIR211-5p and MIR328-3p, induced mitotic failure and proliferation
168 arrest when introduced into primary human melanocytes.
169
170 **Inhibition of AURKB by MIR211-3p and MIR328-5p restricts proliferation in nevi**
171 To investigate the mechanism by which MIR211-5p and MIR328-3p induce arrest in primary human
172 melanocytes, we applied our previously established pipeline for identification of relevant miRNA targets
173 (Fig. 2A)[34]. First, we nucleofected MIR211-5p, MIR328-3p, or control RNA mimics into primary human
174 melanocytes freshly isolated from four independent donors and conducted RNA sequencing (Table S3).
175 We next selected all genes that were significantly downregulated by either miRNA as compared to the
176 control RNA, and further refined the set to the computationally predicted targets of MIR211-5p and/or
177 MIR328-3p. Finally, we nucleofected siRNAs targeting the 115 resulting genes and assayed for reduced
178 EdU incorporation that would phenocopy MIR211-5p or MIR328-3p expression (Table S4). As expected,
179 computationally predicted targets of MIR211-5p and MIR328-3p were enriched in the set of
180 downregulated genes following MIR211-5p or MIR328-3p nucleofection, respectively (Fig. 2B). AURKB,
181 GPR3, and MAPKAPK2 showed the greatest magnitude of repression due to miRNA expression with
182 significance of EdU reduction upon siRNA-mediated knockdown (Fig. 2C). Of these, AURKB (predicted
183 MIR211-5p target) and GPR3 (predicted MIR328-3p target), were significantly inhibited upon
184 nucleofection of either miRNA (Fig. 2D). We reasoned these genes might represent convergent nodes
185 driving proliferation arrest. Further exploration of the AURKB transcript revealed a potential MIR328-3p
186 binding site just before the 3' untranslated region (Fig. 2E). In contrast, we were unable to identify a
187 candidate MIR211-5p binding site in the GPR3 transcript, suggesting indirect inhibition of this gene by
188 MIR211-5p.
189
190
191
192

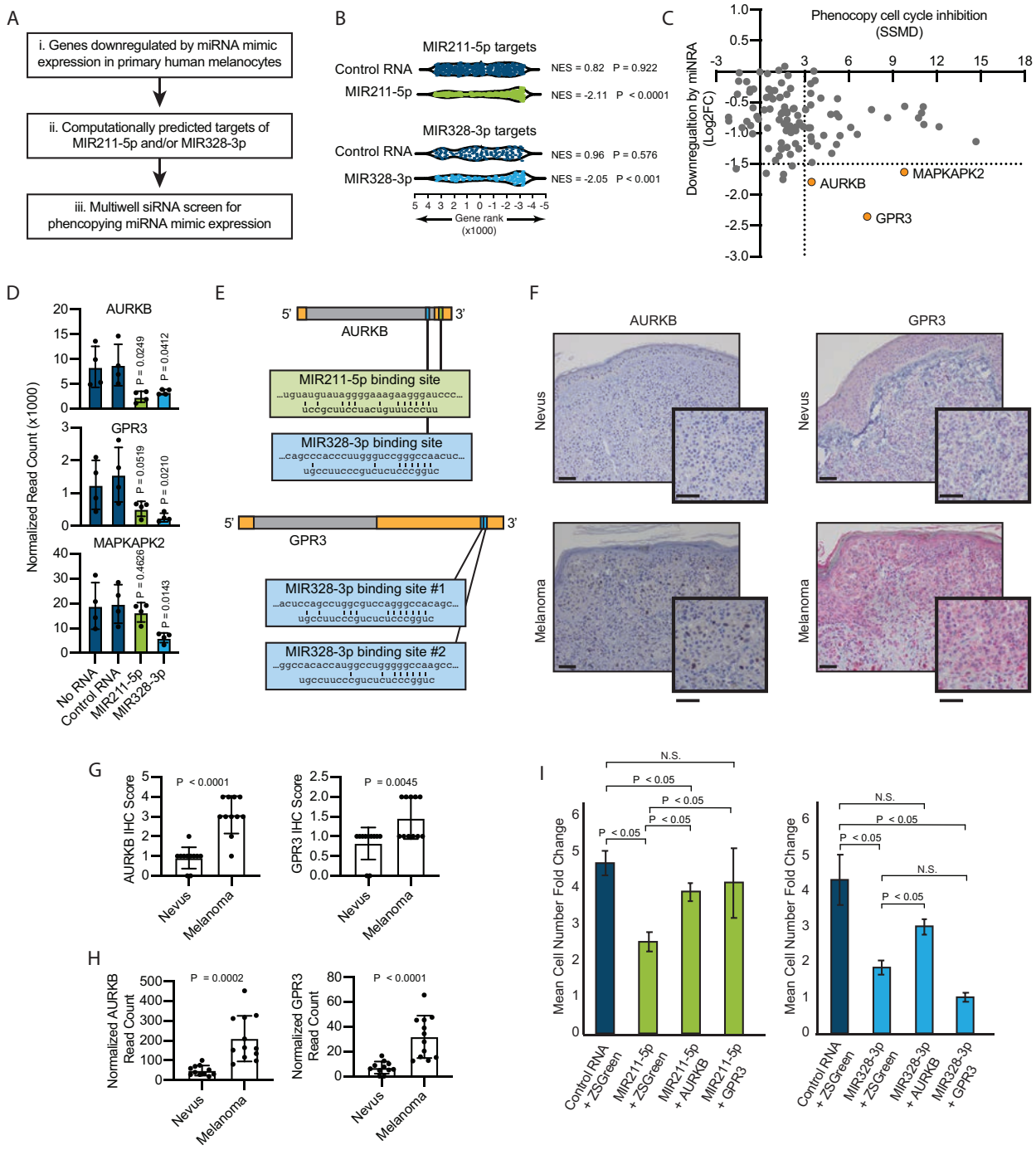

Figure 2

Figure 2: Inhibition of AURKB by MIR211-3p and MIR328-5p restricts proliferation in nevi

(A) Schematic of experimental and computational pipeline for identifying targets of MIR211-3p and/or MIR328-3p responsible for proliferation arrest. **(B)** GSEA analysis comparing predicted MIR211-5p and MIR328-3p target mRNAs to changes in gene expression after nucleofection with indicated mimics compared to nucleofection control. NES = normalized enrichment score. P = nominal P value. Table S3 provides full differentially expressed gene lists. **(C)** Plot of siRNA screen results for phenocopying proliferation arrest versus log2 fold change in expression after miRNA mimic nucleofection. Strictly standardized mean difference (SSMD) reports the magnitude and significance of inhibition of Edu incorporation (n = 3, see

Table S4 for list of genes and screen results). Dotted lines indicate cut-off values for further evaluation. Orange points indicate genes meeting cut-off criteria. **(D)** Mean and standard deviation for expression of indicated genes after nucleofection of indicated mimics (n = 4). P values calculated by unpaired t tests compared to No RNA. **(E)** Schematics showing predicted binding sites of MIR211-5p and MIR328-3p in AURKB and GPR3 transcripts. **(F)** Representative images of immunohistochemical staining for AURKB (brown chromagen) and GPR3 (red chromagen) expression in FFPE samples of nevi and melanoma. **(G)** Mean and standard deviation for immunohistochemical staining scores as in (F) for cohorts of 11 nevi and 11 melanomas. P values calculated by unpaired t tests. **(H)** Mean and standard deviation for read counts for cohorts of 11 nevi and 12 melanomas. P values calculated by unpaired t tests. **(I)** Mean and standard deviation for cell number fold change over 7 days after nucleofection with indicated miRNA mimics in melanocytes transduced with lentiviral constructs expressing zsGreen, AURKB, or GPR3 (n = 6 melanocyte preps, type 2 t test, N.S. = not significant ($P \geq 0.05$)). P values calculated by unpaired t tests.

To determine whether decreased AURKB and/or GPR3 expression was associated with melanocytic nevi, we acquired 23 clinical specimens and measured both the transcript and protein expression of these genes (Fig. 2F-G). The expression of both AURKB and GPR3 protein and mRNA were enriched in melanomas as compared to nevi (Fig. 2G-H). Together, these data demonstrate an inverse expression between two miRNAs (MIR211-5p and MIR328-3p) and two targeted mRNAs (AURKB and GPR3) that toggles concurrently with the transition of arrested melanocytic nevi to melanomas. To further investigate whether either mRNA was sufficient to rescue miRNA-mediated arrest, primary melanocytes were transduced with constructs expressing either zsGreen (control), AURKB or GPR3 (Supplemental File 3) then subsequently nucleofected with either MIR211-5p or MIR328-3p. Expression of either mRNA partially rescued MIR211-5p-induced arrest, while AURKB, but not GPR3, partially rescued MIR328-3p-induced arrest (Fig. 2I). Thus, while other MIR211-5p and MIR328-3p targets, including GPR3, may play a role in the induction of melanocyte proliferation arrest, these data suggest that AURKB inhibition is a critical convergent node of both miRNAs in facilitating proliferation arrest in nevi. This interpretation is further supported by the well-established role of AURKB as an essential orchestrator of successful mitosis[35].

BRAF^{V600E} induces a reversible and conditional proliferation arrest in human melanocytes

We hypothesized that AURKB inhibition by MIR211-5p and MIR328-3p may be the underlying mechanism by which BRAF^{V600E} induces proliferation arrest in melanocytes. BRAF^{V600E} expression has been demonstrated to result in an accumulation of growth-arrested fibroblasts with 2N DNA content, presumably in a permanent G0/G1 senescent state[9,12,17]. In contrast, upon overexpression of MIR211-5p or MIR328-3p, we observed an accumulation of arrested melanocytes with ≥4N DNA content, and a significant decrease in cells with 2N DNA content (Fig. 1L). To determine the DNA content profile of primary human melanocytes under BRAF^{V600E}-induced arrest, we utilized an established lentiviral construct for dose-responsive doxycycline inducible BRAF^{V600E} expression (Fig. 3A)[25]. We monitored melanocyte growth under a titration of doxycycline and identified the lowest concentration (15.6 ng/mL) that induced sustained arrest after 40 hours exposure (Fig. 3B). Similar to our observations for miRNA-

induced arrest, relative per cell dry mass increased by 50% concurrent with BRAF^{V600E} induced- arrest (Fig. 3C). Cell cycle profiling confirmed a significant and dose-dependent accumulation of cells with ≥4N

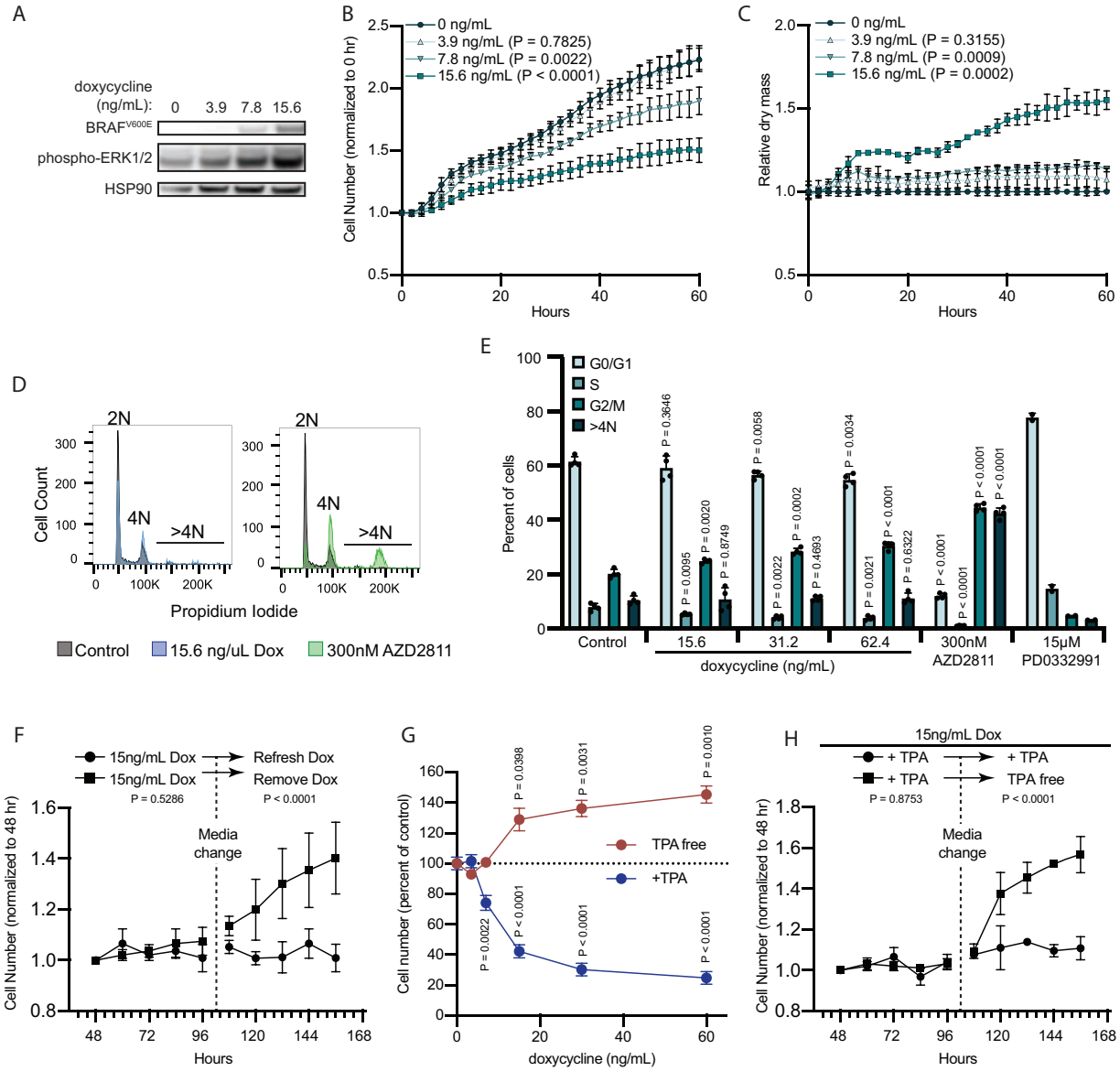

Figure 3

Figure 3: BRAF^{V600E} induces a reversible and conditional arrest in human melanocytes

(A) Representative (of n = 3) Western Blot analysis of BRAF^{V600E}, phospho-ERK1/2, and HSP90 (loading control) in diBRAF^{V600E} melanocytes in response to increasing concentration of doxycycline. **(B)** Mean and standard deviation for relative QPI-derived cell number at indicated hours of diBRAF^{V600E} melanocytes in response to increasing concentration of doxycycline (n = 6). P values from unpaired t tests comparing to 0 ng/mL condition. **(C)** Mean and standard deviation for relative QPI-derived dry mass per cell of diBRAF^{V600E} melanocytes in response to increasing concentration of doxycycline at indicated hours (n = 6). P values from unpaired t tests comparing to 0 ng/mL condition. **(D)** Representative histograms of DNA content profiling via propidium iodide incorporation measured by flow cytometry 5 days after treatment with indicated

molecules. AZD2811 included as a control for induced cytokinesis failure. **(E)** Mean and standard deviation for percent of cells in indicated phases of cell cycle after treatment with doxycycline based upon profiles as in (D) (n = 4). AZD2811 (n = 4) is a control for induced cytokinesis failure. PD0332991 (n = 2) is a control for G0/G1 arrest. P values from unpaired t tests comparing to Control (no treatment) condition. **(F)** Mean and standard deviation for relative QPI-derived cell number of diBRAF^{V600E} melanocytes at indicated hours after treatment doxycycline. Dotted line indicates change in media to either refresh doxycycline or add media without doxycycline (n = 3). P values from unpaired t tests comparing final timepoints. **(G)** Mean and standard deviation for cell number as percent of control of diBRAF^{V600E} melanocytes cultured with or without TPA after 5 days of treatment with indicated concentrations of doxycycline. P values from unpaired t tests comparing to 0 ng/uL condition. **(H)** Mean and standard deviation for relative QPI-derived cell number of diBRAF^{V600E} melanocytes at indicated hours after treatment doxycycline. Dotted line indicates change in media to either refresh TPA-containing media or add media without TPA (n = 3). P values from unpaired t tests comparing final timepoints.

DNA content and a decrease in cells with 2N DNA content (Fig. 3D-E). The cell cycle profiles were notably dissimilar to that of melanocytes treated with a pharmacologic CDK4/6 inhibitor (PD0332991, Palbociclib)[36] known to induce G0/G1 arrest. Treatment with a pharmacologic AURKB inhibitor (AZD2811, Barasertib)[37] that induces G2/M arrest and mitotic failure also resulted in an accumulation of melanocytes with ≥4N DNA content and a decrease in cells with 2N DNA content.

In addition to the accumulation of 2N cells, previous reports of RAF expression in fibroblasts show that transient expression can induce a durable arrest phenotype[17]. To test the durability of BRAF^{V600E}-induced arrest in human melanocytes, we induced doxycylince-dependent BRAF^{V600E} expression for 48 hours and monitored cell number for an additional two days to confirm arrest. Media was then replaced to remove doxycycline. Within twelve hours of doxycycline removal, the previously arrested melanocytes began to proliferate (Fig. 3F), demonstrating that BRAF^{V600E}-induced proliferation arrest in melanocytes is reversible and dependent on continued oncogene expression.

Nevi recurrence after excision[18] and eruption upon external stimuli[19], together with our observation that BRAF^{V600E} induced reversible arrest in melanocytes, suggested that BRAF^{V600E}-induced arrest may dependent on secondary signals from the microenvironment. Tetradecanoylphorbol acetate (TPA) is a protein kinase C (PKC) activator commonly used as a mitogen in primary melanocyte media to substitute for endothelin receptor type B activation[38]. In contrast, TPA also inhibits the cell cycle of melanoma cells[39,40]. BRAF^{V600E} expression permits growth of the Melan-A cell line in the absence of TPA[41]. We therefore wanted to determine the relative contributions of TPA and BRAF^{V600E} to the BRAF^{V600E}-induced primary melanocyte arrest *in vitro*. We induced BRAF^{V600E} expression in primary human melanocytes in two medias – one containing TPA (+TPA) or one containing the endothelin receptor type B ligand, endothelin-1 (TPA-free) and observed divergent dose-responsive phenotypes (Fig. 3G). In the presence of TPA, BRAF^{V600E} expression inhibited cell proliferation. By contrast, in TPA-free media, BRAF^{V600E} expression induced proliferation. We next subjected melanocytes to the arrest inducing conditions of doxycycline treatment in +TPA media for four days, then replaced with doxycycline – containing, TPA-free media. We observed a rapid shift to the proliferative phenotype even in the continued presence of

291 doxycycline (Fig. 3H). From these results, we conclude that BRAF^{V600E} expression induces divergent and
292 interconvertible phenotypes – either hyperproliferation or a reversible arrest – in human melanocytes
293 conditional on extrinsic stimuli.
294
295
296 **BRAF^{V600E}-induced arrest is dependent on melanocyte growth conditions and differentiation state**
297 To investigate the relative contributions of BRAF^{V600E} and TPA to the expression of MIR211-5p and
298 MIR328-3p, we conducted small RNA sequencing of melanocytes grown in +TPA or TPA-free media and
299 with or without BRAF^{V600E} expression. The expression of MIR328-3p was relatively stable, demonstrating
300 less then 2-fold changes across conditions (Fig. 4A-B, Table S5). In contrast, MIR211-5p was one of the
301 most differentially expressed genes in +TPA conditions compared to TPA-free conditions (adj. P = 6.8E-
302 23) (Fig. 4A-B, Table S5). Induction of BRAF^{V600E} in +TPA conditions did not further alter expression of
303 either miRNA. Direct comparison of the arrested melanocytes in +TPA +Dox conditions to the proliferative
304 melanocytes in -TPA +Dox conditions revealed MIR211-5p as the most significantly downregulated
305 miRNA in the proliferative condition (Fig. 4B). Thus, in comparison to TPA, BRAF^{V600E} induction had
306 minimal effect on the expression of the miRNAs. The most notable effect was a decrease of MIR328-3p
307 expression coinciding with the induction of BRAF^{V600E} in TPA free conditions (Fig. 4A). While MIR328-3p
308 downregulation likely contributes to increased proliferation in this condition, the more pronounced effect of
309 TPA on MIR211-5p expression suggests that the mechanisms governing whether BRAF^{V600E} induces
310 arrest or proliferation are a function of the cell's transcriptional state rather than directly downstream of
311 BRAF^{V600E} itself.
312
313 To better characterize the two transcriptional states influencing the BRAF^{V600E} phenotype, we conducted
314 mRNA sequencing of the same specimens. Principal component (PC) analysis revealed that 97.4% of the
315 variance between samples was explained by two principal components – PC1 (81.7% variance)
316 separated transcriptomes based upon exposure to TPA and PC2 (15.7% variance) separated
317 transcriptomes based upon BRAF^{V600E} expression (Fig. 4C, Table S5). We conducted differential
318 expression analyses to compare all samples exposed to +TPA versus TPA-free media, regardless of
319 BRAF^{V600E} expression (Fig. 4D, top) and to compare all samples expressing BRAF^{V600E}, regardless of
320 TPA exposure (Fig. 4D, bottom). As expected from the PC analysis and similar to the miRNA profiles,
321 most gene expression variance was due to media conditions with a smaller, but consistent, set of genes
322 activated by BRAF^{V600E}. We conducted gene set enrichment analyses (GSEA) comparing the TPA
323 regulated genes to known signatures important in human melanocyte or melanoma differentiation[42–44].
324 Signatures associated with differentiation were significantly enriched (NOM P-value < 0.0001) for the
325 genes expressed more highly in TPA-free conditions (Fig. 4E). In contrast, signatures associated with
326 dedifferentiation were significantly enriched (NOM P-value < 0.0001) for the genes expressed more highly

327 in +TPA conditions, together suggesting that exposure to TPA induces a more dedifferentiated phenotype
328 in melanocyte culture.

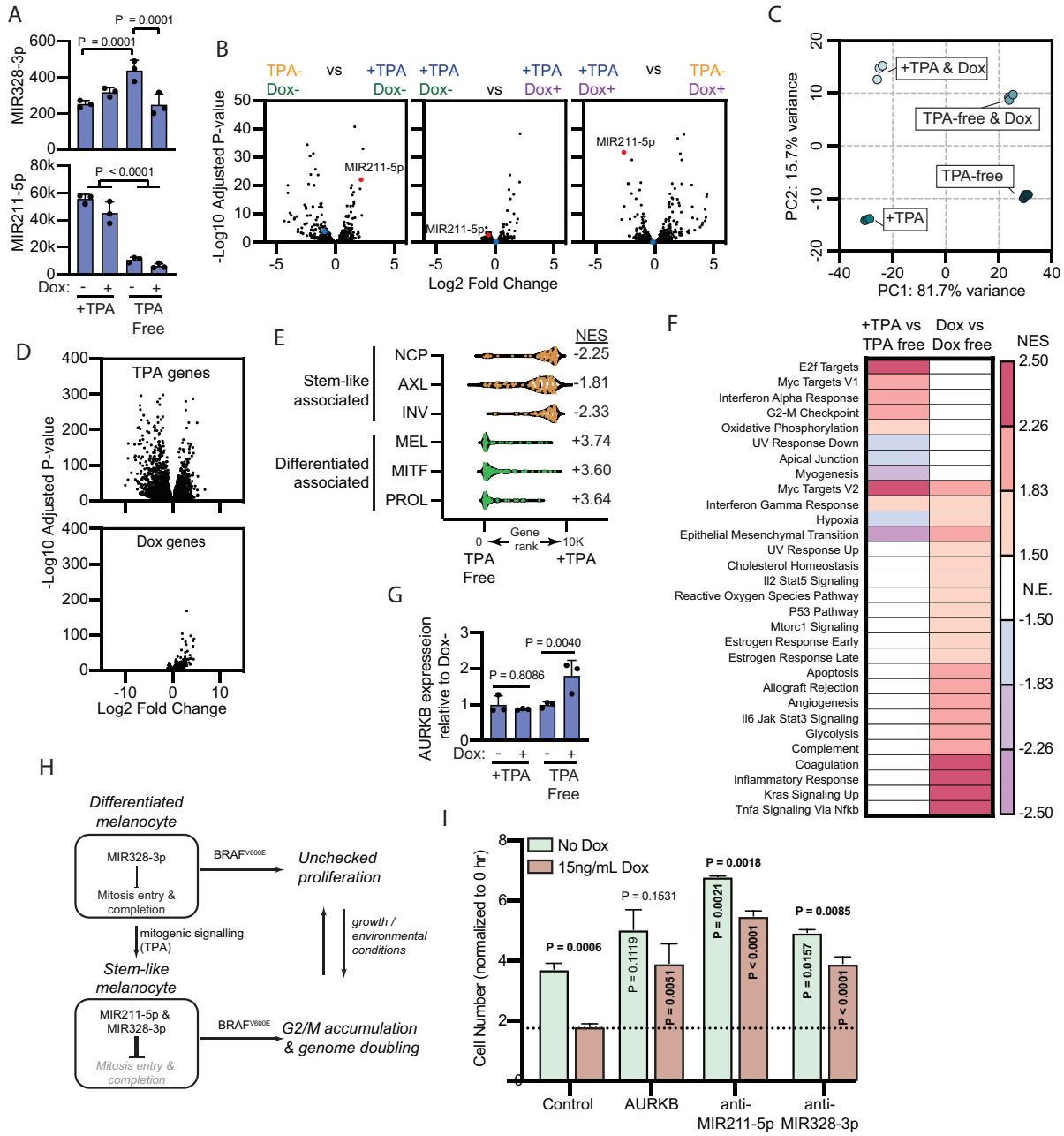

Figure 4

329

330 **Figure 4: BRAF^{V600E}-induced arrest is dependent on melanocyte growth conditions and**
331 **differentiation state**

332 **(A)** Normalized read counts for MIR328-3p (top) and MIR211-5p (bottom) in TPA-containing (+TPA) or TPA-free media,
333 with or without 15.6 ng/mL doxycycline (Dox). See Table S5 for individual values and exact P values. **(B)** Volcano plots
334 depicting log2 fold change against adjusted P value (-Log10) from differential expression (DE) analysis of small RNA
335 sequencing of indicated comparisons. MIR211-5p labelled and shown in red. MIR328-3p shown in blue. **(C)** First and second
336 principal components (PC) separating diBRAF^{V600E} melanocytes cultured in indicated conditions. **(D)** Volcano plots depicting

log2 fold change against adjusted P value (-Log10) from differential expression (DE) analysis of mRNA sequencing of all +TPA specimens versus all TPA-free specimens (top) or all Dox specimens versus all no-Dox specimens (bottom). **(E)** Gene set enrichment analysis (GSEA) comparing DE gene sets from (D) to published signatures of melanocyte differentiation from Tsoi, 2018 (NCP, neural crest progenitors, MEL, differentiated melanocytes); Tirosh, 2016 (AXL, AXL-associated program; MITF, MITF-associated program); Hoek, 2010 (INV, invasive program, PROL, proliferative program). Normalized enrichment score (NES); All NOM P-values < 0.0001. **(F)** GSEA comparing DE genes sets from (D) to Hallmark gene sets. Only significant enrichments (NES > 1.5 or NES < -1.5 and NOM P-value < 0.01) shown. **(G)** Normalized read counts for AURKB normalized to no Dox conditions (n = 3). P values from unpaired t tests. Sequencing data represented in A-G from n=3 per condition analyzed with DESeq2. **(H)** Schematic of model supported by transcriptomic analyses. TPA induces a more stem-like state in human melanocytes. Due to increased f MIR211-5p and base-line MIR328-3p expression, $BRAF^{V600E}$ does not induce AURKB, resulting in G2/M accumulation. **(I)** Mean and standard deviation for cell number as percent of time point 0 hr after 7 days of culture in +TPA media with or without 15.6 ng/mL Dox (n = 3 per condition). Melanocytes were transduced with either pLVX-control, -AURKB, -anti-MIR211-5p, or -anti-MIR328-3p. P values from unpaired t tests comparing to matched no Dox condition (horizontal), Control no Dox condition (vertical in green bar) or Control Dox condition (vertical in red bar).

To identify biological processes associated with differentially expressed genes we conducted GSEAs to compare TPA-regulated genes and $BRAF^{V600E}$- regulated genes to the Molecular Signature Database Hallmark gene sets[45]. Despite fewer over-all differentially expressed genes, we observed a greater number of enriched pathways among the $BRAF^{V600E}$- regulated genes (absolute NES > 1.5, NOM P-value <0.01) (Fig. 4F). Among the enriched pathways were the expected increases in MAPK (KRAS) signaling, glycolysis[46], and MTOR signaling[47]. Among the few enriched pathways of TPA- regulated genes were gene sets associated with increased proliferation (MYC and E2F Targets) and, intriguingly, with the G2-M Checkpoint. Combined with our observation that $BRAF^{V600E}$-induced proliferation arrest is +TPA dependent and characterized by cells with ≥4N DNA content (Fig. 3E), this result suggests that stimulating growth in +TPA conditions results in accumulation of cells in the G2/M phase of the cell cycle.

One initially surprising result of this analysis was the static expression of both MIR211-5p and MIR328-3p in +TPA conditions, regardless of $BRAF^{V600E}$ expression. However, as inhibitors of translation, miRNA function depends on the expression level of its targets[48,49], effectively functioning as buffers of gene expression that prevent aberrantly high levels of a transcript[50]. $BRAF^{V600E}$ has been previously demonstrated as an upstream activator of AURKB transcription in melanoma cells[51]. We therefore reasoned that MIR211-5p expression in +TPA conditions might dampen AURKB activation by $BRAF^{V600E}$. Consistent with this hypothesis, the addition of doxycycline induced AURKB expression in TPA-free / MIR211-5p low conditions, but this effect was not observed in +TPA / MIR211-5p high conditions (Fig. 4G).

Collectively, our transcriptomic analyses support a model whereby growth in +TPA conditions induces a more dedifferentiated state in melanocytes coinciding with an increase in MIR211-5p expression (Fig. 4H). This increased MIR211-5p combined with relatively stable MIR328-3p expression, dampens entry

377 into mitosis and/or successful completion of mitosis at least in part through AURKB inhibition. The
378 attenuation of cell division results in an accumulation of cells in G2/M – an effect that is more pronounced
379 in conditions stimulating accelerated growth, such as with $BRAF^{V600E}$ expression. To test this model, we
380 transduced doxycycline-inducible $BRAF^{V600E}$ melanocytes in +TPA conditions with lentiviral constructs
381 constitutively expressing either AURKB (Supplemental File 2A) or miRNA sponges (Supplemental File
382 2D) to either MIR211-5p or MIR328-3p. AURKB expression had no baseline effect on melanocyte growth,
383 but rescued $BRAF^{V600E}$-induced arrest (Fig. 4I), suggesting the inability of the oncogene to induce AURKB
384 in this context serves as a bottleneck in cell division. Also consistent with the model, sponges against
385 either MIR211-5p or MIR328-3p increased baseline division rate and rescued $BRAF^{V600E}$-induced arrest,
386 demonstrating that both miRNAs contribute to inhibition of melanocyte division, with affects that are more
387 pronounced in the presence of growth signals.
388
389 **AURKB inhibition drives melanocytic nevus-associated proliferation arrest**
390 To further investigate whether this mechanism of arrest occurs in clinical nevus specimens, we examined
391 an independent cohort of 15 nevi for evidence of mitotic failure. Histopathologic analysis revealed that all
392 nevi within the cohort exhibited binucleation (Fig. 5A). The percent observed binucleated melanocytes
393 ranged from 3-12% (mean = 6.3%). It is important to note that since binucleation can only be observed in
394 the fraction of cells sectioned perpendicular to the plane of the adjacent nuclei, 3-12% is likely an under-
395 estimate. We also observed giant multinucleated cells in 10 of the 15 nevi, indicative of multiple rounds of
396 DNA synthesis and cytokinetic failure and consistent with previous reports[52].
397
398 We sought to determine whether AURKB inhibition was necessary and sufficient for the multi-nucleated
399 arrest we observed in melanocytic nevi. We obtained three fresh skin biopsies containing nevi,
400 microdissected the nevus portion, and isolated melanocytes (Fig. 5B). Nevus-derived melanocytes
401 appeared healthy in culture. Consistent with the histopathologic cohort, co-staining with melanocyte
402 marker, MLANA, and Hoechst revealed frequent 4N and 8N melanocytes (Fig. 5C). Transduction of
403 nevus melanocytes with an AURKB and mCherry expressing lentiviral vector at low multiplicity of infection
404 (MOI) showed that the mCherry positive cells divided significantly more than the their mCherry negative
405 counterparts (Fig. 5d-e) in cells from all three nevus donors. This result suggests that expression of
406 AURKB is also rate limiting for the proliferation of human nevus melanocytes, as we observed in primary
407 melanocytes expressing $BRAF^{V600E}$.
408
409 To test the sufficiency of AURKB inhibition to limit $BRAF^{V600E}$ hyperproliferation in melanoma, we
410 assessed normalized growth rate inhibition of three cultures - primary human melanocytes, an
411 established $BRAF^{V600E}$ human melanoma cell line, and a short-term $BRAF^{V600E}$ human melanoma culture
412 - when exposed to a pharmacologic AURKB inhibitor (Barasertib). Normalized growth rate measurements
413 (such as GR_{50}) are independent of baseline cell division rate and are demonstrably more reproducible

than the classically calculated half maximal inhibitor concentration (IC_{50}) when comparing different cell cultures[53]. An additional advantage of GR_{50} is the ability to distinguish growth rate inhibition (GR_{50} approaches 0) versus cell death (GR_{50} is negative). Since GR_{50} calculations require proliferation curves,

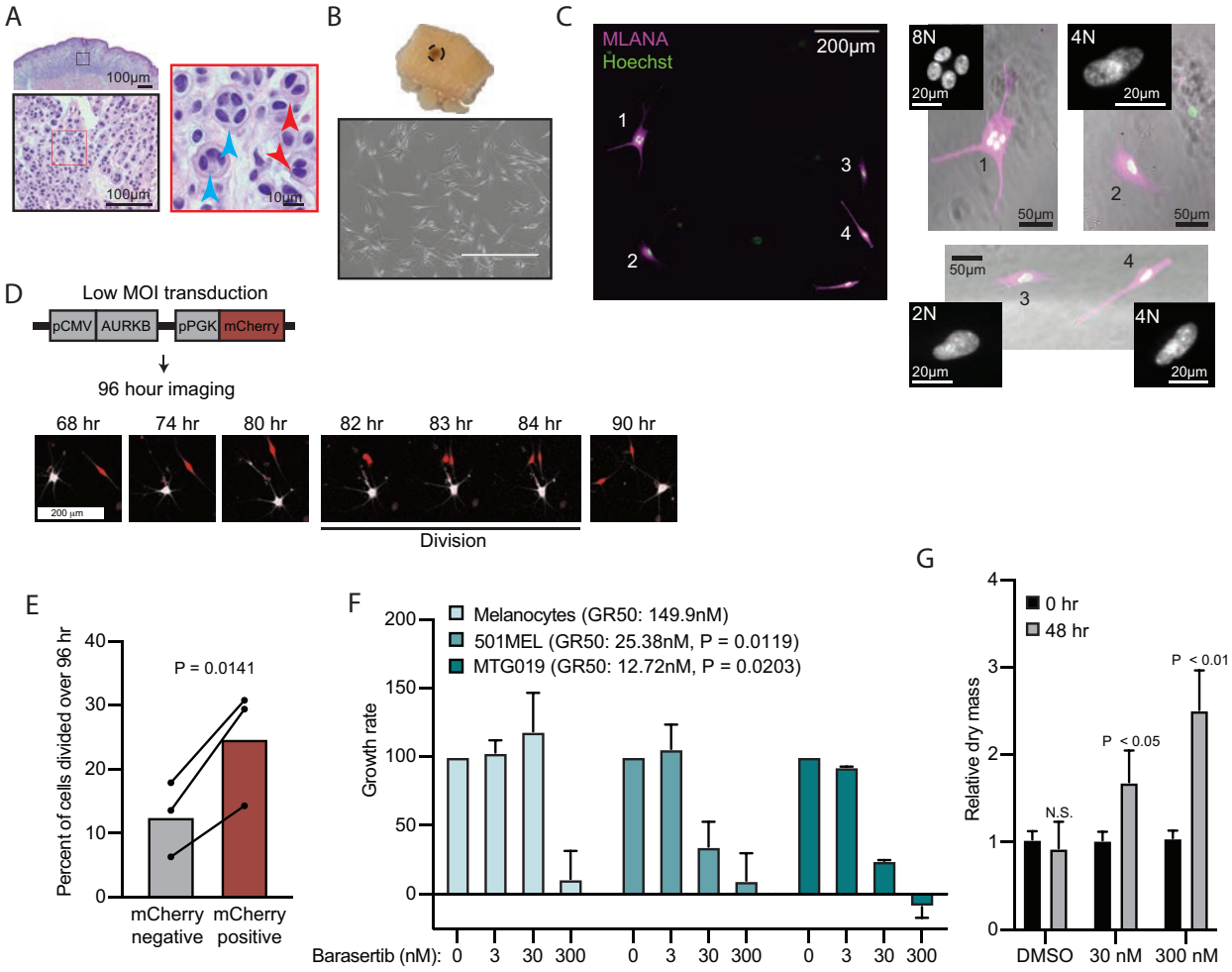

Figure 5

Figure 5: AURKB inhibition is critical for BRAF^{V600E}-induced arrest of human nevi

(A) Representative image of 15 H&E-stained melanocytic nevus. Border colors indicate two consecutive magnifications. Arrowheads indicate bi- (red) or multi- (blue) nucleation. **(B)** Example images of skin specimen containing a melanocytic nevus (circled) and phase contrast microscopy of melanocytes isolated from nevus portion. **(C)** Images of MLANA (purple) and Hoeschst (green) co-staining of melanocytic nevus derived melanocytes in culture. Zoomed images show representative 2N, 4N, and 8N cells. **(D)** Representative of images of QPI coupled with fluorescence microscopy to identify adjacent mCherry -expressing and mCherry-negative melanocytes. Individual cells were identified at time zero, tracked and monitored for division for 96 hrs. **(E)** Mean and individual matched datapoints for the percent of n = 3 mCherry-negative or mCherry-positive cells identified at time zero that divided over 96 hrs. P value from paired t test. **(F)** Mean and standard deviation for 48 hr growth rates of indicated cells treated with Barasertib. P values from unpaired t tests comparing the 30nM samples of melanoma lines to primary melanocytes (n = 3). **(G)** Mean and standard deviation for relative QPI-derived dry mass per 501MEL cell at initial time point (black) compared to 48 hr treatment with Barasertib (grey) (n = 3). P values from unpaired t tests.

we conducted live QPI over 48 hours with a range of Barasertib concentrations (0-300nM). Primary melanocytes were largely resistant to the compound with reduced growth apparent only at supraphysiological levels (Fig. 5f). In contrast, both melanoma cultures responded to ten-fold lower dosage of the compound with GR_{50} approaching zero, indicating primarily arrest, not death. In these conditions, the per cell dry mass also increased significantly, consistent with a G2/M arrest (Fig. 5g). Taken together, these data demonstrate that AURKB inhibition limits the rate of $BRAF^{V600E}$-induced proliferation in human melanocytic nevi and melanomas.

Discussion

Cellular senescence is conventionally defined as a permanent cell-cycle arrest associated with a variety of molecular markers and an irreversible arrest in the G0/G1 phase of the cell cycle[10–12]. The vast majority of melanocytic nevi are stably arrested and harbor $BRAF^{V600E}$, an oncogenic mutation that induces cellular senescence when expressed in a variety of mammalian cells[9,12,17]. While these observations seemingly implicate OIS as the mechanism driving nevus- associated proliferation arrest, a substantial body of evidence has challenged this paradigm in recent years[8,9,18–25]. Here, we uncover an alternative mechanism driving nevus formation and stability whereby acquisition of the $BRAF^{V600E}$ mutation does not necessitate proliferation arrest, but instead permits melanocytes to toggle between hyperproliferation and arrest. Our transcriptomic analyses suggest that external stimuli can modulate the differentiation state of $BRAF^{V600E}$ melanocytes, orchestrate the expression level of MIR211-5p, and inform which phenotype is triggered by the oncogene – before or after the oncogene is introduced. Our data suggest that hyperproliferation requires AURKB – a kinase necessary for successful cytokinesis that is directly downstream of $BRAF^{V600E}$ [54]. Whereas sufficient levels of AURKB permit proliferation, AURKB suppression by MIR211-5p and MIR328-3p results in mitotic failure.

The presented model offers an explanation for several clinical phenomena. First, melanocytic nevi form when $BRAF^{V600E}$ drives hyperproliferation followed by proliferation arrest. Second, nevus eruption involves expansion of previously stable nevi over a short period of time. Interestingly, nevus eruption has been observed in metastatic melanoma patients treated with single agent selective BRAF inhibitors[55–59], consistent with our observation that proliferation arrest in melanocytes requires sustained expression of the oncogene. Third, incomplete excision of melanocytic nevi can result in subsequent regrowth of the benign lesion[18]. Each event requires modulation of the $BRAF^{V600E}$ melanocyte between a proliferative and arrested phase. Our data demonstrate that $BRAF^{V600E}$ melanocytes can indeed induce proliferative or arrested states and is consistent with each of these events.

Diminished MIR211-5p/MIR328-3p expression concurrent with increased AURKB expression occurs in a substantial portion of melanomas. AURKB expression was previously reported as significantly elevated in

469 melanoma metastases[51] and here we report increased expression in primary melanomas. Similarly,
470 MIR211-5p expression is consistently observed as lost in melanoma as compared to melanocytic nevi
471 across independent studies[27–29]. Indeed, MIR211-5p expression levels classify nevi from melanomas with
472 a high degree of accuracy[27,28]. We have reported on the diagnostic potential of MIR328-3p expression as
473 well, although multi-study validation was impeded by the absence of hybridization probes in earlier
474 microarray-based profiling datasets[28]. *In vitro*, we have now demonstrated that inhibition of either miRNA
475 is sufficient to block BRAF^{V600E}-induced arrest in melanocytes. These data suggest that mitotic failure
476 serves as a barrier to melanoma progression and is consistent with the genome duplication and copy
477 number alterations associated with invasive melanoma[4,60]. In melanoma, the specific cause of this
478 genomic instability is unknown, but reentry of cells into cell cycle after mitotic failure has been shown to
479 cause genome duplication and accumulation of copy number alterations in other cancers[61]. Further
480 experiments will be necessary to determine whether dysregulation the spindle checkpoint in nevi
481 contributes directly to the copy number variations present in melanomas.
482
483 It is important to note that while our data support a model of reversible proliferation arrest in nevi, it does
484 not suggest this reversal is commonplace. Unquestionably, the vast majority of melanocytic nevi present
485 with sustained arrest. However, we do propose that the duration of arrest is dynamic and modulated by
486 exposure to external signals. Since our data suggest that loss of MIR211-5p and MIR328-3p expression
487 and restoration of AURKB expression is concurrent with progression to melanoma, identification of the
488 source of cell-extrinsic signals might suggest new strategies for chemoprevention or therapy. We have
489 identified TPA, a known activator of PKC signaling, as one extrinsic factor that induces expression of
490 MIR211-5p and a more dedifferentiated state. Previous studies have identified TPA as either a mitogen,
491 inhibitor of the G1/S transition, or inhibitor of the G2/M transition, dependent on the context[39,40,62–64]. We
492 demonstrate that *in vitro*, TPA activation of MIR211-5p is required for BRAF^{V600E}-induced mitotic failure.
493 Yet, the inclusion of TPA in primary melanocyte culture is artificial and the environmental stimulus that
494 regulates MIR211-5p expression in skin remains unknown. One hypothesis is that PKC activation from
495 keratinocyte interactions serves as the extrinsic stimulus. However, TPA-free media containing an
496 endothelin receptor type B ligand, endothelin-1, did not elicit MIR211-5p expression or BRAF^{V600E} arrest,
497 suggestive that the downstream signaling pathways regulated by the two molecules are not identical.
498 PKC activation can also result in increased MAPK signaling[65,66] raising the possibility that internal MAPK
499 fluctuations may play a role in toggling between BRAF^{V600E}-induced proliferation versus arrest. MIR211-
500 5p is also reported to be transcriptionally regulated by both MITF[67] and UV exposure[68]. Additionally,
501 autocrine signaling might be at play, such that melanocyte density triggers the arrested state as predicted
502 by recent mathematic modeling of nevus formation[8]. An important future direction will be to identify the
503 nature and physiological source of this signal for melanocytic nevi in human skin.
504

505 In summary, we have identified that BRAF^{V600E} induces a reversible and conditional arrest in human
506 melanocytes orchestrated by MIR211-5p/MIR328-3p regulation of AURKB. We present a mechanistic
507 model that allows for melanocytic nevus formation, eruption and recurrence. Moreover, our observations
508 provide an explanation for the genetic duplication and instability inherent to invasive melanomas and
509 open new directions for novel chemopreventative and therapeutic strategies.
510
511 **Competing Interests**
512 R.L.J and M.L.W are inventors on international patent application no. PCT/US2019/023834 concerning
513 the use of microRNAs investigated in this article as molecular diagnostics for melanoma.
514
515 **Acknowledgments**
516 This work was supported by the National Institutes of Health (DP5OD019787 to R.L.J., 5F31CA236377 to
517 A.S.M., P30CA042014 to University of Utah) and the University of California, San Francisco Program for
518 Breakthrough Biomedical Research (PBBR) Sandler Fellowship to R.L.J. We acknowledge the use of the
519 HCI Shared Resources for Research Informatics (RI), Cancer Biostatistics (CB), High-Throughput
520 Genomics and Bioinformatics Analysis (GBA), and the Biorepository and Molecular Pathology (BMP)
521 Research Histology Section supported by P30CA042014 awarded to HCI from the National Cancer
522 Institute.
523
524 **Author Contributions**
525 A.S.M: Investigation, Formal analysis, Writing – original draft, Visualization, Funding acquisition; R.L.B.:
526 Methodology, Investigation, Resources, Writing – review & editing; H.Z.: Methodology, Investigation,
527 Validation, Writing – review & editing; K.B.: Investigation; R.T.: Formal analysis; M.C. – Formal analysis;
528 A.H.S.: Data curation, Writing – review & editing; R.A., Writing – review & editing: Resources; S.H.:
529 Conceptualization; D.H.L.: Conceptualization, Writing – review & editing; T.H.M.: Resources; M.W.V.:
530 Conceptualization; D.G.: Resources, Writing – review & editing; M.W.: Resources, Writing – review &
531 editing; U.E.L.: Investigation, Formal Analysis, Resources, Writing – review & editing; R.L.J.:
532 Conceptualization, Formal analysis, Investigation, Writing – original draft; Visualization, Supervision,
533 Funding acquisition.
534
535 **Materials and Methods**
536
537 *Transcriptomic profiling*
538 For FFPE samples, histopathologic review, microdissection, targeted exon sequencing, phylogenetic
539 analysis, and RNA and small RNA sequencing of each tumor area were previously described
540 (phs001550.v2.p1)[23,26,28]. For this study, small RNA reads were aligned to human reference (hg37) with
541 Bowtie[69] and small RNA reference groups (miRBase21) were counted. For mRNA sequencing, reads

542 were aligned to human reference (hg37) with Bowtie2 and counted with HTSeq. Differential expression
543 analysis was performed using DESeq2[70] with p-values adjusted by Benjamini-Hochberg method (p-adj).
544 Previously published RNA sequencing datasets from *Shain et al. 2018* and *Torres, et al.* 2020 were re-
545 analyzed here with DESeq2 the combined for visualization. For RNA profiling from primary melanocytes,
546 total RNA was extracted using TRIzol Reagent (Thermo Fisher, 15596-026) and further purified with the
547 RNeasy Power Clean Pro Cleanup Kit (Qiagen, 13997-50) to remove melanin. For small RNAseq of
548 nevus melanocytes sequencing libraries were constructed with the TailorMix Small RNA Library
549 Preparation Kit (SeqMatic, CA) and sequencing was performed on the Illumina HiSeq2500 platform at
550 single-end 50bp. For small RNAseq of cultured $BRAF^{V600E}$ transduced melanocytes, sequencing libraries
551 were constructed with the Qiagen QIAseq miRNA Library Prep kit and sequencing was performed on the
552 NovaSeq SP platform at paired-end 50bp. For mRNAseq of microRNA mimic nucleofected melanocytes,
553 150bp paired end sequencing was conducted by GeneWiz. For mRNAseq of cultured $BRAF^{V600E}$
554 transduced melanocytes, sequencing libraries were constructed with the Illumina TruSeq Stranded mRNA
555 Library Prep kit and sequencing was performed on the NovaSeq S4 platform at paired-end 150bp.
556
557 *Cell derivation and culture*
558 Benign human melanocytic nevi were excised with informed consent from patient donors at the UCSF
559 Dermatology clinic (San Francisco, CA) or HCI Dermatology clinic according to Institutional Review
560 Board- approved protocols. Nevus tissue was minced and enzymatically dissociated in 1mg/mL
561 collagenase (Sigma 11213857001) and 3.3mg/mL dispase (Sigma, 4942078001) in DMEM (Thermo
562 Fisher, 10569044) for 1 hour at 37ºC. Melanocytes were further isolated by 5- day exposure to 10µg/mL
563 G418 (InvivoGen, ant-gn-1). BRAF status was confirmed via sanger sequencing (Quintarabio) using the
564 primer set: BRAF forward: 5'- GCA CGA CAG ACT GCA CAG GG -3'; BRAF reverse: 5'- AGC GGG CCA
565 GCA GCT CAA TAG -3'. BRAF wildtype (normal) human melanocytes were isolated from de-identified
566 and IRB consented neonatal foreskins or adult skin. Foreskin tissue was incubated overnight at 4ºC in
567 dispase and epithelia were mechanically separated from the dermis the following morning. Epithelial
568 tissue was minced and incubated in 0.25% trypsin (Gibco 25200056) for 4min at 37ºC. Trypsin was
569 quenched and tissue centrifuged at 500xg for 5min at room temperature. The cell/tissue pellet was
570 resuspended in Melanocyte medium (ThermoFisher, M254500) with HMGS (ThermoFisher, S0025) and
571 plated in low volume.
572
573 The 501Mel human melanoma line (Gift from Dr. Boris Bastian, CVCL_4633) were cultured in RPMI with
574 10% Fetal Bovine Serum (FBS, VWR, S107G), 1% Penicillin-Streptomycin (Gibco, 15140122), 1% L-
575 Glutamine (Gibco, 25030149), and 1% Non-Essential Amino Acids (Gibco, 11140050). HCIMel019 was
576 derived from patient-derived xenograft (PDX) tumors propagated in mice. An HCIMel019 (P2)
577 subcutaneous tumor was resected from mouse, minced in digestion buffer (100µM HEPES (Gibco,
578 15630-080), 5% FBS (DENVILLE, FB5001-H), 20µg/ml gentamicin (Gibco, 15710-064), 1x insulin (Gibco,

579 51500-056), and 1mg/ml collagenase IV (Gibco, 17104-019) in DMEM (Gibco, 11965-092)), and digested
580 overnight at 37˚C. Cells were filtered through a 100µm filter (Falcon, 352360) and red blood cells
581 removed with RBC lysis buffer (0.5M EDTA, 0.5M KHCO3 (Sigma, 237205), and 5M NH4CL (Sigma,
582 A9434)). Remaining cells were washed with PBS (Gibco, 10010023), and cultured at 37ºC and 5% CO2
583 in Mel2 media consisting of 80%MCDB153 (Sigma, M7403), 20% L15 (Gibco, 11415-064), 2% FBS
584 (DENVILLE, FB5001-H), 1.68mM CaCL (Sigma, C4901), 1x insulin (Gibco, 51500-056) 5ng/ml EGF
585 (Sigma Aldrich, E9644), 15µg/ml Bovine Pituitary Extract (Gibco 13028-014), and 1x Pen/strep (Gibco,
586 15070-063).
587
588 *Small RNA Nucleofection*
589 Human melanocytes were trypsinized (Gibco, 25300062), quenched, and centrifuged at 300xg. Cells
590 were resuspended in R Buffer (ThermoFisher, MPK1025) at 10,000 cells/µL. 10µL of cell slurry was
591 mixed with miRIDIAN microRNA mimics (Dharmacon: hsa-MIR211-5p C-300566-03-0005, hsa-MIR328-
592 3p C-300695-03-0005, MIRControl 1 CN-001000-01-05 or MIRControl 2 CN-002000-01-05); or On-
593 TargetPlus siRNA (Dharmacon, custom library); at 4µM final concentration and nucleofected using the
594 NEON Transfection System and protocol (Thermo Fisher, MPK5000).
595
596 *Generation of Lentiviral vectors*
597 pTRIPZ-diBRAFV600E was a gift from Todd Ridky[25]. pLVX-AURKB (Addgene #153316) and pLVX-
598 GPR3 (Addgene #153317) were generated by subcloning the respective human cDNA (from Addgene
599 #100142 and #66350) into the MluI and BamHI sites] of the pLVX-Che-hi3 vector (a gift of Sanford
600 Simon)[71]. pLVX-anti-MIR211-5p (Addgene #153318), pLVX-anti-MIR328-3p (Addgene #153319), and
601 pLVX-Che-zsGreen (Addgene #153320) were generated by inserting zsGreen with or without a 3'UTR
602 into the MluI and XbaI sites of the pLVX-Che-hi3 vector. The 3'UTRs contained 7 tandem microRNA
603 binding sites to report and inhibit microRNA function, as previously described[34]. ZsGreen was subcloned
604 from pHIV-zsGreen (gift from Bryan Welm & Zena Werb (Addgene #18121))[72].
605
606 *Lentiviral transduction*
607 $2.75x10^6$ HEK293T cells were plated on 10cm tissue culture dishes and grown for ~24 hours in DMEM
608 with 10% FBS. For each 10cm plate, 5µg lentiviral vector, 3.3µg of pMLV-GagPol and 1.7µg of pVSV-G
609 packaging plasmids were added to 500µL of jetPRIME buffer and 20µL of jetPRIME transfection reagent
610 (Polyplus, 712-60), and transfected according to manufacturer's instructions. 48 hours post-transfection,
611 viral supernatant was collected and filtered using 0.45µm syringe filters (Argos 4395-91). Human
612 melanocytes seeded at $1.0x10^5$ – $2.0x10^5$ cells/well density in 6-well plates were incubated in viral
613 supernatant with 10µg/mL polybrene (Sigma, TR-1003) and centrifuged at 300xg for 60 min at room
614 temperature. The viral supernatant was removed and replaced with growth media. Transduced cells were
615 either selected with puromycin (1µg/mL for 5 days, Sigma P8833) or sorted for mCherry expression using

616 a BD FACSAria II. Cells expressing pTRIPZ-diBRAFV600E were treated with doxycycline (Sigma, D9891)
617 at indicated concentrations.
618
619 *Live Quantitative Phase Imaging*
620 Live quantitative imaging was performed using either the HoloMonitor M4 imaging cytometers (Phase
621 Holographic Imaging, Lund, Sweden) or the Livecyte platform (Phasefocus, Sheffield, UK). Analyses of
622 cell proliferation, dry cell mass, and death were acquired with the M4 platform and analyzed using
623 HStudio (v2.6.3) as previously described[31]. For each experiment, human melanocytes were seeded into
624 6-well plates (Sarstedt, 83.3920) at 100,000 cells/well and either live-imaged or serially imaged as
625 indicated. Analysis of growth rate were acquired with the M4 platform and analyzed using App Suite
626 (v3.2.0.60) as previously described[53]. For each experiment, 100,000 melanocytes, 60,000 501Mel cells or
627 150,000 HCIMel019 cells were plated per well and media containing indicated concentrations of
628 barasertib (AURKB inhibitor; AZD1152-HQPA | AZD2811, Selleckchem, A1147) was added. Cells were
629 imaged for 48-72 hours. Analyses of fluorescent reporters coupled with quantitative phase imaging was
630 conducted using the Livecyte platform and analyzed using Analyze (v3.1) (Phasefocus, Sheffield, UK).
631
632 *EdU assays*
633 Normal human melanocytes were nucleofected with microRNA mimics, LNA microRNA inhibitors, or
634 infected with lentiviral vectors (as above) and seeded in 48-well plates at a density of 50,000 cells/well. 4
635 days post-seeding EdU was added to culture media at a 10μM final concentration. 24 hours after EdU
636 addition, media was removed and cells were stained for EdU incorporation and nuclei using the Click-iT
637 EdU Imaging Kit (Thermo Fisher, C10337) and protocol. Images of EdU and nuclei staining were
638 acquired using the Evos FL microscope and quantified with FIJI.
639
640 *Western Blotting*
641 Protein was collected using RIPA Buffer (Thermo Fisher, 89901) supplemented with HALT Protease
642 Inhibitor (Thermo Fisher, 87786). Immunoblotting was carried out as previously described[23]. Membranes
643 were incubated overnight at 4 °C with primary antibodies at the following dilutions: anti-HSP90 (CST,
644 4874) 1:1000, anti-BRAFV600E (Spring Bioscience Corp, E19292) 1:1000, anti-phosphoERK1/2 (CST,
645 4970) 1:1000, anti-AURKB (Abcam, ab2254) 1:1000. Membranes were washed 4X with TBS and 0.5%
646 Tween20, incubated with HRP-conjugated secondary antibody (1:2000) for 30 minutes at room
647 temperature, and visualized with Lumina Forte Western HRP substrate (Millipore, WBLUF0500).
648
649 *DNA content and apoptosis profiling*
650 For assessing DNA content, trypsinized melanocytes (as above) were resuspended in 400 PBS. 1mL -20
651 ºC 200 proof ethanol was added dropwise while gently vortexing to achieve 70% final concentration for
652 fixation and incubated overnight at -30 ºC. Cells were centrifuged at 800xg for 5 min, washed with fresh

653 PBS, and incubated in 500µL FxCycle PI/RNase Staining Solution (Invitrogen, F10797) for 20 min at 37
654 ºC. Data were collected on the Fortessa (BD) at low speed and analyzed with FlowJo v10.7.1. Annexin
655 V/PI staining was performed by trypsinizing melanocytes as above. Cells were washed with PBS and
656 resuspended with Annexin V binding buffer (BioLegend, 422201) at a concentration of 1X10^6 cell/mL.
657 5µL APC Annexin V antibody (BioLegend, 640919) and 10µL PI were added. Cells were gently vortexed
658 and incubated in the dark at room temperature for 15 min. Cells were resuspended in 400µL of Annexin
659 V Binding Buffer. Data were collected on the FACs Verse (BD) and analyzed with FlowJo v10.7.1.
660
661 *Human nevus and melanoma tissue immunohistochemistry*
662 The archived clinical specimens used in the study were procured with IRB approval from the UCSF
663 Dermatopathology Pathology Service archives. For assessment of AURKB and GPR3 expression, 11
664 melanoma and 11 melanocytic nevi with previous diagnosis were de-identified and re-verified
665 histologically (UEL). For assessment of DNA content, 15 additional melanocytic nevi with previous
666 diagnosis were re-verified histologically (UEL). Tissue was fixed in 10% neutral-buffered formalin,
667 processed, embedded in paraffin, and stained with hematoxylin and eosin. 4µm FFPE sections were
668 stained with AURKB (1:400 dilution, Abcam ab2254) or GPR3 (1:125 dilution, Abnova H00002827-M01)
669 antibodies. UEL reviewed immunohistochemical stains with semiquantitative grading for GPR3 (0=none;
670 1=patchy positive; 2=strong positive) and AURKB (0=none; 1=rare positive; 2=scattered positive; 3=
671 frequent positive; 4=many positive).
672
673 *Statistical analyses*
674 For differential gene expression, p values were calculated with the DESeq2 (v1.30.1) default Wald test
675 adjusted by the Benjamini-Hochberg method using a 5% false discovery rate (FDR)[73]. Pathway analyses
676 were analyzed using the fast gene set enrichment package[74] in R with a 10% FDR. Gene set enrichment
677 analyses were conducted using GSEA (v4.0.3, Broad Institute) Preranked tool with 1000 permutations.
678 For *in vitro* experiments, pilot studies were initially conducted in triplicate. The required minimal sample
679 size to assess the difference between independent means with independent standard deviations with an
680 alpha error probability of 0.05 and a power of 0.95 was calculated using G*Power (v. 3.1.9.4). P-values
681 were calculated using either paired or unpaired two-tailed T Tests or Wilcoxon tests via Prism 8
682 (Graphpad) as indicated in figure legends.
683
684 *Experimental set-up*
685 For cohorts of clinical specimens, sample number (n) refers to the number of specimens, each from a
686 different patient. For *in vitro* experiments, n refers to independent experiments conducted on different
687 days. In cases where fresh primary melanocytes were used, the cells in each experiment are derived from
688 an independent donor. In cases where cell lines are used, the cells in each experiment represent a
689 different passage and/or day of that line. For different conditions within experiments, replicate wells were

690 plated and arbitrarily chosen for each condition (e.g. not treated versus treated; different concentrations of
691 a compounds, etc.). All data were included.
692
693 *Ethics statement*
694 The archived clinical specimens used in the study were procured with IRB approval from the UCSF
695 Dermatopathology Pathology Service archives (11-07951). Fresh human tissue samples used in this
696 study were obtained with informed consent and consent to publish from each patient. Samples were first
697 coded before being provided to the researchers. The study protocol conformed to the ethical guidelines of
698 the Declaration of Helsinki (1975). Samples were processed following standard operating procedures
699 approved by IRB at University of California, San Francisco (16-20299) and at the Huntsman Cancer
700 Institute (00124195).
701
702 *Data availability*
703 The data which support these findings are available within the article and its supplementary files, as well
704 as from the corresponding author upon reasonable request. The sequencing data produced in this
705 manuscript is available from GEO under the accession number GSE150849.
706
707 **References**
708
709 1. Garnett MJ, Marais R. Guilty as charged: B-RAF is a human oncogene. Cancer Cell.
710 2004;6(4):313–9.
711 2. Davies H, Bignell GR, Cox C, Stephens P, Edkins S, Clegg S, Teague J, Woffendin H, Garnett
712 MJ, Bottomley W, Davis N, Dicks E, Ewing R, Floyd Y, Gray K, Hall S, Hawes R, Hughes J,
713 Kosmidou V, Menzies A, Mould C, Parker A, Stevens C, Watt S, Hooper S, Jayatilake H,
714 Gusterson BA, Cooper C, Shipley J, Hargrave D, Pritchard-Jones K, Maitland N, Chenevix-Trench
715 G, Riggins GJ, Bigner DD, Palmieri G, Cossu A, Flanagan A, Nicholson A, Ho JWC, Leung SY,
716 Yuen ST, Weber BL, Seigler HF, Darrow TL, Paterson H, Wooster R, Stratton MR, Futreal PA.
717 Mutations of the BRAF gene in human cancer. Nature. Nature; 2002 Jun 27 [cited 2021 Mar
718 1];417(6892):949–954.
719 3. Pollock PM, Harper UL, Hansen KS, Yudt LM, Stark M, Robbins CM, Moses TY, Hostetter G,
720 Wagner U, Kakareka J, Salem G, Pohida T, Heenan P, Duray P, Kallioniemi O, Hayward NK,
721 Trent JM, Meltzer PS. High frequency of BRAF mutations in nevi. Nat Genet. Nat Genet; 2003 Jan
722 1 [cited 2021 Mar 1];33(1):19–20.
723 4. Shain AH, Yeh I, Kovalyshyn I, Sriharan A, Talevich E, Gagnon A, Dummer R, North J, Pincus L,
724 Ruben B, Rickaby W, D'Arrigo C, Robson A, Bastian BC. The Genetic Evolution of Melanoma
725 from Precursor Lesions. N Engl J Med. Massachussetts Medical Society; 2015 Nov 12 [cited 2020
726 Jun 27];373(20):1926–1936.

727 5. Bastian BC. The molecular pathology of melanoma: An integrated taxonomy of melanocytic
728 neoplasia. Annu Rev Pathol Mech Dis. Annual Reviews Inc.; 2014 [cited 2020 Aug 21];9:239–271.
729 6. Dankort D, Curley DP, Cartlidge RA, Nelson B, Karnezis AN, Damsky Jr WE, You MJ, DePinho
730 RA, McMahon M, Bosenberg M. BrafV600E cooperates with Pten loss to induce metastatic
731 melanoma. Nat Genet. 2009 May 12 [cited 2019 Jul 17];41(5):544–552.
732 7. Damsky W, Micevic G, Meeth K, Muthusamy V, Curley DP, Santhanakrishnan M, Erdelyi I, Platt
733 JT, Huang L, Theodosakis N, Raza Zaidi M, Tighe S, Davies MA, Dankort D, McMahon M, Merlino
734 G, Bardeesy N, Bosenberg M. mTORC1 activation blocks brafV600E-induced growth arrest but is
735 insufficient for melanoma formation. Cancer Cell. Cell Press; 2015;27(1):41–56.
736 8. Ruiz-Vega R, Chen CF, Razzak E, Vasudeva P, Krasieva TB, Shiu J, Caldwell MG, Yan H,
737 Lowengrub J, Ganesan AK, Lander AD. Dynamics of nevus development implicate cell
738 cooperation in the growth arrest of transformed melanocytes. Elife. eLife Sciences Publications
739 Ltd; 2020 Oct 1 [cited 2021 Mar 1];9:1–24.
740 9. Michaloglou C, Vredeveld LCW, Soengas MS, Denoyelle C, Kuilman T, van der Horst CMAM,
741 Majoor DM, Shay JW, Mooi WJ, Peeper DS. BRAFE600-associated senescence-like cell cycle
742 arrest of human naevi. Nature. 2005 Aug 4 [cited 2019 Jul 17];436(7051):720–724.
743 10. He S, Sharpless NE. Senescence in Health and Disease [Internet]. Cell. Cell Press; 2017 [cited
744 2021 Mar 2]. p. 1000–1011.
745 11. Roy AL, Sierra F, Howcroft K, Singer DS, Sharpless N, Hodes RJ, Wilder EL, Anderson JM. A
746 Blueprint for Characterizing Senescence. Cell. Cell Press; 2020 Nov 25 [cited 2021 Mar
747 2];183(5):1143–1146.
748 12. Serrano M, Lin AW, McCurrach ME, Beach D, Lowe SW. Oncogenic ras provokes premature cell
749 senescence associated with accumulation of p53 and p16(INK4a). Cell. Cell Press; 1997 Mar 7
750 [cited 2021 Mar 2];88(5):593–602.
751 13. Campisi J, D'Adda Di Fagagna F. Cellular senescence: When bad things happen to good cells
752 [Internet]. Nature Reviews Molecular Cell Biology. Nat Rev Mol Cell Biol; 2007 [cited 2021 Mar 2].
753 p. 729–740.
754 14. Collado M, Serrano M. The power and the promise of oncogene-induced senescence markers
755 [Internet]. Nature Reviews Cancer. Nat Rev Cancer; 2006 [cited 2021 Mar 2]. p. 472–476.
756 15. Afshari CA, Vojta PJ, Annab LA, Futreal PA, Willard TB, Barrett JC. Investigation of the role of
757 G1/S cell cycle mediators in cellular senescence. Exp Cell Res. Exp Cell Res; 1993 [cited 2021
758 Mar 2];209(2):231–237.
759 16. Chatsirisupachai K, Palmer D, Ferreira S, de Magalhães JP. A human tissue-specific
760 transcriptomic analysis reveals a complex relationship between aging, cancer, and cellular
761 senescence. Aging Cell. Blackwell Publishing Ltd; 2019 Dec 1 [cited 2021 Mar 2];18(6).
762 17. Zhu J, Woods D, McMahon M, Bishop JM. Senescence of human fibroblasts induced by
763 oncogenic Raf. Genes Dev. Cold Spring Harbor Laboratory Press; 1998 Oct 1 [cited 2021 Mar

764 1];12(19):2997–3007.
765 18. King R, Hayzen BA, Page RN, Googe PB, Zeagler D, Mihm MC. Recurrent nevus phenomenon: A
766 clinicopathologic study of 357 cases and histologic comparison with melanoma with regression.
767 Mod Pathol. Mod Pathol; 2009 May [cited 2021 Mar 2];22(5):611–617.
768 19. Burian EA, Jemec GBE. Eruptive Melanocytic Nevi: A Review. Am J Clin Dermatol. 2019 May 22
769 [cited 2019 Jun 21];20(5):669–682.
770 20. Cotter MA, Florell SR, Leachman SA, Grossman D. Absence of senescence-associated β-
771 galactosidase activity in human melanocytic nevi in vivo [3] [Internet]. Journal of Investigative
772 Dermatology. J Invest Dermatol; 2007 [cited 2021 Mar 2]. p. 2469–2471.
773 21. Tran SL, Haferkamp S, Scurr LL, Gowrishankar K, Becker TM, Desilva C, Thompson JF, Scolyer
774 RA, Kefford RF, Rizos H. Absence of distinguishing senescence traits in human melanocytic nevi.
775 J Invest Dermatol. Nature Publishing Group; 2012 [cited 2021 Mar 2];132(9):2226–2234.
776 22. Oaxaca G, Billings SD, Ko JS. p16 Range of expression in dermal predominant benign epithelioid
777 and spindled nevi and melanoma. J Cutan Pathol. Blackwell Publishing Ltd; 2020 Sep 6 [cited
778 2021 Mar 2];47(9):815–823.
779 23. Zeng H, Jorapur A, Shain AH, Lang UE, Torres R, Zhang Y, McNeal AS, Botton T, Lin J, Donne
780 M, Bastian IN, Yu R, North JP, Pincus L, Ruben BS, Joseph NM, Yeh I, Bastian BC, Judson RL.
781 Bi-allelic Loss of CDKN2A Initiates Melanoma Invasion via BRN2 Activation. Cancer Cell. Cell
782 Press; 2018 Jul 9 [cited 2021 Mar 2];34(1):56-68.e9.
783 24. Haferkamp S, Scurr LL, Becker TM, Frausto M, Kefford RF, Rizos H. Oncogene-induced
784 senescence does not require the p16 INK4a or p14ARF melanoma tumor suppressors. J Invest
785 Dermatol. J Invest Dermatol; 2009 Aug [cited 2021 Mar 2];129(8):1983–1991.
786 25. McNeal AS, Liu K, Nakhate V, Natale CA, Duperret EK, Capell BC, Dentchev T, Berger SL, Herlyn
787 M, Seykora JT, Ridky TW. CDKN2B loss promotes progression from benign melanocytic nevus to
788 melanoma. Cancer Discov. American Association for Cancer Research Inc.; 2015 Oct 1 [cited
789 2021 Mar 2];5(10):1072–1085.
790 26. Shain AH, Joseph NM, Yu R, Benhamida J, Liu S, Prow T, Ruben B, North J, Pincus L, Yeh I,
791 Judson R, Bastian BC. Genomic and Transcriptomic Analysis Reveals Incremental Disruption of
792 Key Signaling Pathways during Melanoma Evolution. Cancer Cell. 2018 Jul 9 [cited 2019 Jul
793 17];34(1):45-55.e4.
794 27. Babapoor S, Horwich M, Wu R, Levinson S, Gandhi M, Makkar H, Kristjansson A, Chang M,
795 Dadras SS. microRNA in situ hybridization for miR-211 detection as an ancillary test in melanoma
796 diagnosis. Mod Pathol. Nature Publishing Group; 2016 May 1 [cited 2021 Apr 27];29(5):461–475.
797 28. Torres R, Lang UE, Hejna M, Shelton SJ, Joseph NM, Shain AH, Yeh I, Wei ML, Oldham MC,
798 Bastian BC, Judson-Torres RL. MicroRNA Ratios Distinguish Melanomas from Nevi. J Invest
799 Dermatol. Elsevier B.V.; 2020 Jan 1 [cited 2021 Mar 9];140(1):164-173.e7.
800 29. Latchana N, Ganju A, Howard JH, Carson WE. MicroRNA dysregulation in melanoma. Surg

801 Oncol. Elsevier Ltd; 2016 Sep 1 [cited 2021 Mar 9];25(3):184–189.
802 30. Miniotis MF, Mukwaya A, Wingren AG. Digital holographic microscopy for non-invasive monitoring
803 of cell cycle arrest in L929 cells. PLoS One. Public Library of Science; 2014 Sep 1 [cited 2021 Mar
804 9];9(9).
805 31. Hejna M, Jorapur A, Song JS, Judson RL. High accuracy label-free classification of single-cell
806 kinetic states from holographic cytometry of human melanoma cells. Sci Rep. Nature Publishing
807 Group; 2017 Dec 1 [cited 2021 Mar 9];7(1).
808 32. Barker KL, Boucher KM, Judson-Torres RL. Label-Free Classification of Apoptosis, Ferroptosis
809 and Necroptosis Using Digital Holographic Cytometry. Appl Sci. MDPI AG; 2020 Jun 27 [cited
810 2021 Mar 9];10(13):4439.
811 33. Normand G, King RW. Understanding cytokinesis failure. Adv Exp Med Biol. NIH Public Access;
812 2010 [cited 2021 Mar 9];675:27–55.
813 34. Judson RL, Greve TS, Parchem RJ, Blelloch R. MicroRNA-based discovery of barriers to
814 dedifferentiation of fibroblasts to pluripotent stem cells. Nat Struct Mol Biol. Nat Struct Mol Biol;
815 2013 Oct [cited 2020 Aug 30];20(10):1227–1237.
816 35. D'Avino PP, Capalbo L. New auroras on the roles of the chromosomal passenger complex in
817 cytokinesis: Implications for cancer therapies. Front Oncol. Frontiers Media S.A.; 2015 [cited 2021
818 Mar 9];5(OCT).
819 36. Clark AS, Karasic TB, DeMichele A, Vaughn DJ, O'Hara M, Perini R, Zhang P, Lal P, Feldman M,
820 Gallagher M, O'Dwyer PJ. Palbociclib (PD0332991) - A selective and potent cyclin-dependent
821 kinase inhibitor: A review of pharmacodynamics and clinical development [Internet]. JAMA
822 Oncology. American Medical Association; 2016 [cited 2021 Mar 9]. p. 253–260.
823 37. Helfrich BA, Kim J, Gao D, Chan DC, Zhang Z, Tan AC, Bunn PA. Barasertib (AZD1152), a small
824 molecule Aurora B inhibitor, inhibits the growth of SCLC cell lines in vitro and in vivo. Mol Cancer
825 Ther. American Association for Cancer Research Inc.; 2016 Oct 1;15(10):2314–2322.
826 38. Hsu MY, Li L, Herlyn M. Cultivation of normal human epidermal melanocytes in the absence of
827 phorbol esters. Methods Mol Med. Methods Mol Med; 2005 [cited 2021 May 6];107:13–28.
828 39. Coppock DL, Buffolino P, Kopman C, Nathanson L. Inhibition of the melanoma cell cycle and
829 regulation at the G1/S transition by 12-O-tetradecanoylphorbol-13-acetate (TPA) by modulation of
830 CDK2 activity. Exp Cell Res. 1995 Nov [cited 2021 May 6];221(1):92–102.
831 40. Arita Y, Buffolino P, Coppock DL. Regulation of the cell cycle at the G2/M boundary in metastatic
832 melanoma cells by 12-O-tetradecanoyl phorbol-13-acetate (TPA) by blocking p34(cdc2) kinase
833 activity. Exp Cell Res. Academic Press Inc.; 1998 Aug 1 [cited 2021 May 6];242(2):381–390.
834 41. Wellbrock C, Ogilvie L, Hedley D, Karasarides M, Martin J, Niculescu-Duvaz D, Springer CJ,
835 Marais R. V599EB-RAF is an Oncogene in Melanocytes. Cancer Res. Cancer Res; 2004 Apr 1
836 [cited 2021 Mar 9];64(7):2338–2342.
837 42. Hoek KS, Goding CR. Cancer stem cells versus phenotype-switching in melanoma [Internet].

838 Pigment Cell and Melanoma Research. Pigment Cell Melanoma Res; 2010 [cited 2021 May 6]. p.
839 746–759.
840 43. Tirosh I, Izar B, Prakadan SM, Wadsworth MH, Treacy D, Trombetta JJ, Rotem A, Rodman C,
841 Lian C, Murphy G, Fallahi-Sichani M, Dutton-Regester K, Lin JR, Cohen O, Shah P, Lu D,
842 Genshaft AS, Hughes TK, Ziegler CGK, Kazer SW, Gaillard A, Kolb KE, Villani AC, Johannessen
843 CM, Andreev AY, Van Allen EM, Bertagnolli M, Sorger PK, Sullivan RJ, Flaherty KT, Frederick DT,
844 Jané-Valbuena J, Yoon CH, Rozenblatt-Rosen O, Shalek AK, Regev A, Garraway LA. Dissecting
845 the multicellular ecosystem of metastatic melanoma by single-cell RNA-seq. Science (80-).
846 American Association for the Advancement of Science; 2016 Apr 8 [cited 2021 May
847 6];352(6282):189–196.
848 44. Tsoi J, Robert L, Paraiso K, Galvan C, Sheu KM, Lay J, Wong DJL, Atefi M, Shirazi R, Wang X,
849 Braas D, Grasso CS, Palaskas N, Ribas A, Graeber TG. Multi-stage Differentiation Defines
850 Melanoma Subtypes with Differential Vulnerability to Drug-Induced Iron-Dependent Oxidative
851 Stress. Cancer Cell. Cell Press; 2018 May 14 [cited 2021 May 6];33(5):890-904.e5.
852 45. Liberzon A, Birger C, Thorvaldsdóttir H, Ghandi M, Mesirov JP, Tamayo P. The Molecular
853 Signatures Database Hallmark Gene Set Collection. Cell Syst. Cell Press; 2015 Dec 23 [cited
854 2021 May 6];1(6):417–425.
855 46. Haq R, Fisher DE, Widlund HR. Molecular pathways: BRAF induces bioenergetic adaptation by
856 attenuating oxidative phosphorylation. Clin Cancer Res. American Association for Cancer
857 Research Inc.; 2014 May 1 [cited 2021 May 6];20(9):2257–2263.
858 47. Prabowo AS, Iyer AM, Veersema TJ, Anink JJ, Schouten-Van Meeteren AYN, Spliet WGM, Van
859 Rijen PC, Ferrier CH, Capper D, Thom M, Aronica E. BRAF V600E mutation is associated with
860 mTOR signaling activation in glioneuronal tumors. Brain Pathol. Brain Pathol; 2014 Jan [cited
861 2021 May 6];24(1):52–66.
862 48. Mukherji S, Ebert MS, Zheng GXY, Tsang JS, Sharp PA, Van Oudenaarden A. MicroRNAs can
863 generate thresholds in target gene expression. Nat Genet. Nat Genet; 2011 Sep [cited 2021 May
864 6];43(9):854–859.
865 49. Ovando-Vázquez C, Lepe-Soltero D, Abreu-Goodger C. Improving microRNA target prediction
866 with gene expression profiles. BMC Genomics. BioMed Central Ltd.; 2016 May 17 [cited 2021 May
867 6];17(1).
868 50. Ebert MS, Sharp PA. Roles for MicroRNAs in conferring robustness to biological processes
869 [Internet]. Cell. Elsevier B.V.; 2012 [cited 2021 May 6]. p. 515–524.
870 51. Sharma A, Madhunapantula S V., Gowda R, Berg A, Neves RI, Robertson GP. Identification of
871 Aurora Kinase B and Wee1-Like Protein Kinase as Downstream Targets of V600EB-RAF in
872 Melanoma. Am J Pathol. Am J Pathol; 2013 Apr [cited 2021 Apr 27];182(4):1151–1162.
873 52. Rogers T, Marino ML, Raciti P, Jain M, Busam KJ, Marchetti MA, Marghoob AA. Biologically
874 distinct subsets of nevi [Internet]. Giornale Italiano di Dermatologia e Venereologia. Edizioni

875 Minerva Medica; 2016 [cited 2021 Apr 27]. p. 365–384.
876 53. Hafner M, Niepel M, Chung M, Sorger PK. Growth rate inhibition metrics correct for confounders in
877 measuring sensitivity to cancer drugs. Nat Methods. Nature Publishing Group; 2016 Jun 1 [cited
878 2021 Mar 8];13(6):521–527.
879 54. Bonet C, Giuliano S, Ohanna M, Bille K, Allegra M, Lacour JP, Bahadoran P, Rocchi S, Ballotti R,
880 Bertolotto C. Aurora B is regulated by the mitogen-activated protein kinase/extracellular signal-
881 regulated kinase (MAPK/ERK) signaling pathway and is a valuable potential target in melanoma
882 cells. J Biol Chem. J Biol Chem; 2012 Aug 24 [cited 2021 Mar 10];287(35):29887–29898.
883 55. Cohen PR, Bedikian AY, Kim KB. Appearance of New Vemurafenib-associated Melanocytic Nevi
884 on Normal-appearing Skin: Case Series and a Review of Changing or New Pigmented Lesions in
885 Patients with Metastatic Malignant Melanoma After Initiating Treatment with Vemurafenib. J Clin
886 Aesthet Dermatol. Matrix Medical Communications; 2013 May [cited 2021 Apr 27];6(5):27–37.
887 56. Chen FW, Tseng D, Reddy S, Daud AI, Swetter SM. Involution of eruptive melanocytic nevi on
888 combination BRAF and MEK inhibitor therapy. JAMA Dermatology. American Medical Association;
889 2014 Nov 1 [cited 2021 Apr 27];150(11):1209–1212.
890 57. Chu EY, Wanat KA, Miller CJ, Amaravadi RK, Fecher LA, Brose MS, McGettigan S, Giles LR,
891 Schuchter LM, Seykora JT, Rosenbach M. Diverse cutaneous side effects associated with BRAF
892 inhibitor therapy: A clinicopathologic study. J Am Acad Dermatol. J Am Acad Dermatol; 2012 Dec
893 [cited 2021 Apr 27];67(6):1265–1272.
894 58. Dalle S, Poulalhon N, Debarbieux S, Zaharia D, Mihm MC, Lacouture ME, Rosen A, Marghoob
895 AA, Busam KJ, Depaepe L, Bringuier PP, Richez P, Baurain JF, Bressac-de Paillerets B, Balme B,
896 Thomas L. Tracking of second primary melanomas in vemurafenib-treated patients. JAMA
897 Dermatology. JAMA Dermatol; 2013 Apr [cited 2021 Apr 27];149(4):488–490.
898 59. Zimmer L, Hillen U, Livingstone E, Lacouture ME, Busam K, Carvajal RD, Egberts F, Hauschild A,
899 Kashani-Sabet M, Goldinger SM, Dummer R, Long G V., McArthur G, Scherag A, Sucker A,
900 Schadendorf D. Atypical melanocytic proliferations and new primary melanomas in patients with
901 advanced melanoma undergoing selective BRAF Inhibition. J Clin Oncol. J Clin Oncol; 2012 Jul 1
902 [cited 2021 Apr 27];30(19):2375–2383.
903 60. Vergara IA, Mintoff CP, Sandhu S, McIntosh L, Young RJ, Wong SQ, Colebatch A, Cameron DL,
904 Kwon JL, Wolfe R, Peng A, Ellul J, Dou X, Fedele C, Boyle S, Arnau GM, Raleigh J, Hatzimihalis
905 A, Szeto P, Mooi J, Widmer DS, Cheng PF, Amann V, Dummer R, Hayward N, Wilmott J, Scolyer
906 RA, Cho RJ, Bowtell D, Thorne H, Alsop K, Cordner S, Woodford N, Leditschke J, O'Brien P,
907 Dawson SJ, McArthur GA, Mann GJ, Levesque MP, Papenfuss AT, Shackleton M. Evolution of
908 late-stage metastatic melanoma is dominated by aneuploidy and whole genome doubling. Nat
909 Commun. Nature Research; 2021 Dec 1 [cited 2021 May 12];12(1).
910 61. Telentschak S, Soliwoda M, Nohroudi K, Addicks K, Klinz FJ. Cytokinesis failure and successful
911 multipolar mitoses drive aneuploidy in glioblastoma cells. Oncol Rep. Spandidos Publications;

912 2015 Apr 1 [cited 2021 Mar 9];33(4):2001–2008.
913 62. Arita Y, O'Driscoll KR, Weinstein IB. Growth of Human Melanocyte Cultures Supported by 12-0-
914 Tetradecanoylphorbol-13-acetate Is Mediated through Protein Kinase C Activation. Cancer Res.
915 1992 [cited 2021 May 6];52(16):4514–4521.
916 63. Stavroulaki M, Kardassis D, Chatzaki E, Sakellaris G, Lindschau C, Haller H, Tosca A, Krasagakis
917 K. Exposure of normal human melanocytes to a tumor promoting phorbol ester reverses growth
918 suppression by transforming growth factor beta. J Cell Physiol. J Cell Physiol; 2008 Feb [cited
919 2021 May 6];214(2):363–370.
920 64. Chao-Hsing KAO, Hsin-Su YU. A study of the effects of phorbol 12-myristate-13-acetate on cell
921 differentiation of pure human melanocytes in vitro. Arch Dermatol Res. Springer-Verlag; 1991 Apr
922 [cited 2021 May 6];283(2):119–124.
923 65. Herrera R, Hubbell S, Decker S, Petruzzelli L. A role for the MEK/MAPK pathway in PMA-induced
924 cell cycle arrest: Modulation of megakaryocytic differentiation of K562 cells. Exp Cell Res.
925 Academic Press Inc.; 1998 Feb 1 [cited 2021 Apr 26];238(2):407–414.
926 66. Ueda Y, Hirai SI, Osada SI, Suzuki A, Mizuno K, Ohno S. Protein kinase C δ activates the MEK-
927 ERK pathway in a manner independent of Ras and dependent on Raf. J Biol Chem. J Biol Chem;
928 1996 [cited 2021 May 6];271(38):23512–23519.
929 67. Mazar J, de Young K, Khaitan D, Meister E, Almodovar A, Goydos J, Ray A, Perera RJ. The
930 Regulation of miRNA-211 Expression and Its Role in Melanoma Cell Invasiveness. PLoS One.
931 PLoS One; 2010 [cited 2021 Apr 27];5(11).
932 68. Su M, Miao F, Jiang S, Shi Y, Luo L, He X, Wan J, Xu S, Lei TC. Role of the
933 p53-TRPM1/miR-211-MMP9 axis in UVB-induced human melanocyte migration and its potential in
934 repigmentation. Int J Mol Med. Spandidos Publications; 2020 [cited 2021 Apr 27];45(4):1017–
935 1026.
936 69. Langmead B, Trapnell C, Pop M, Salzberg SL. Ultrafast and memory-efficient alignment of short
937 DNA sequences to the human genome. Genome Biol. Genome Biol; 2009 Mar 4 [cited 2021 Apr
938 27];10(3).
939 70. Love MI, Huber W, Anders S. Moderated estimation of fold change and dispersion for RNA-seq
940 data with DESeq2. Genome Biol. BioMed Central Ltd.; 2014 Dec 5 [cited 2021 Apr 27];15(12).
941 71. Takacs CN, Andreo U, Dao Thi VL, Wu X, Gleason CE, Itano MS, Spitz-Becker GS, Belote RL,
942 Hedin BR, Scull MA, Rice CM, Simon SM. Differential Regulation of Lipoprotein and Hepatitis C
943 Virus Secretion by Rab1b. Cell Rep. Elsevier B.V.; 2017 Oct 10 [cited 2021 Apr 27];21(2):431–
944 441.
945 72. Welm BE, Dijkgraaf GJP, Bledau AS, Welm AL, Werb Z. Lentiviral Transduction of Mammary
946 Stem Cells for Analysis of Gene Function during Development and Cancer. Cell Stem Cell. Cell
947 Stem Cell; 2008 Jan 10 [cited 2021 Apr 27];2(1):90–102.
948 73. Benjamini Y, Drai D, Elmer G, Kafkafi N, Golani I. Controlling the false discovery rate in behavior

genetics research. Behav Brain Res. Behav Brain Res; 2001 [cited 2021 May 12]. p. 279–284.

74. Korotkevich G, Sukhov V, Budin N, Shpak B, Artyomov M, Sergushichev A. Fast gene set enrichment analysis. bioRxiv. Cold Spring Harbor Laboratory; 2016 Oct 22 [cited 2021 May 12];060012.

Supplemental Files and Legends

Supplemental File 1 (related to Figure 1 and Supplemental File 2)

4 day time-lapse quantitative phase imaging of cytokinesis failure in primary melanocytes transduced with MIR211-5p. Annotations provided in Figure S1.

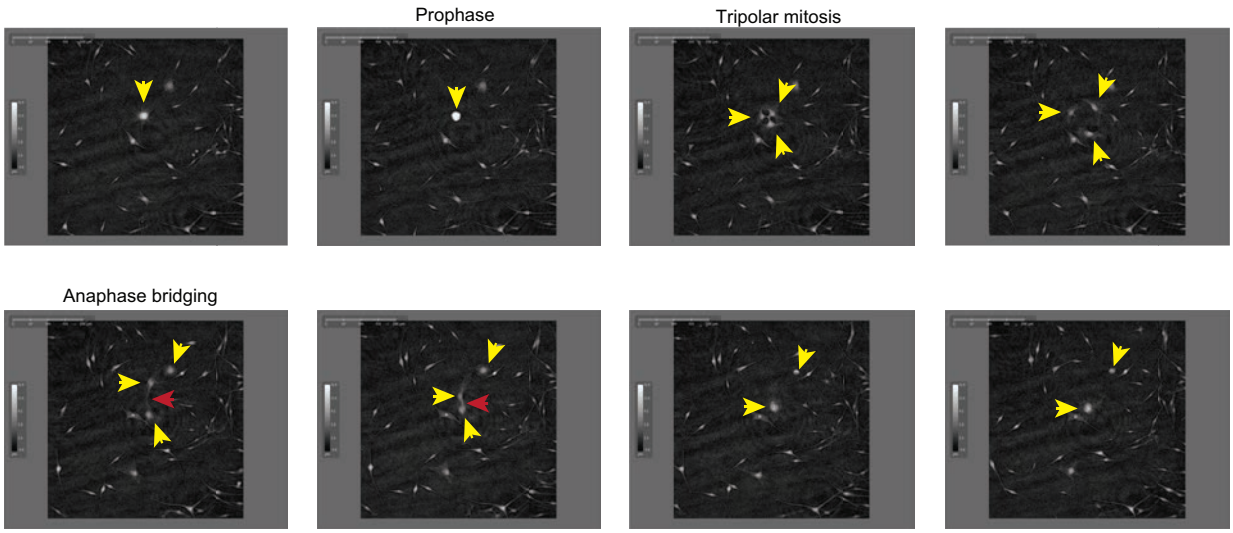

Supplemental Figure S1

Supplemental File 2 (related to Figure 1 and Supplemental File 1)

Still frames from Supplemental Video 1 documenting representative cytokinesis failure in primary melanocytes transduced with MIR211-5p. Yellow arrow heads follow a single cell and its progeny through a tripolar mitosis. Red arrow head follows an anaphase bridge connecting two daughter cells that then remerge.

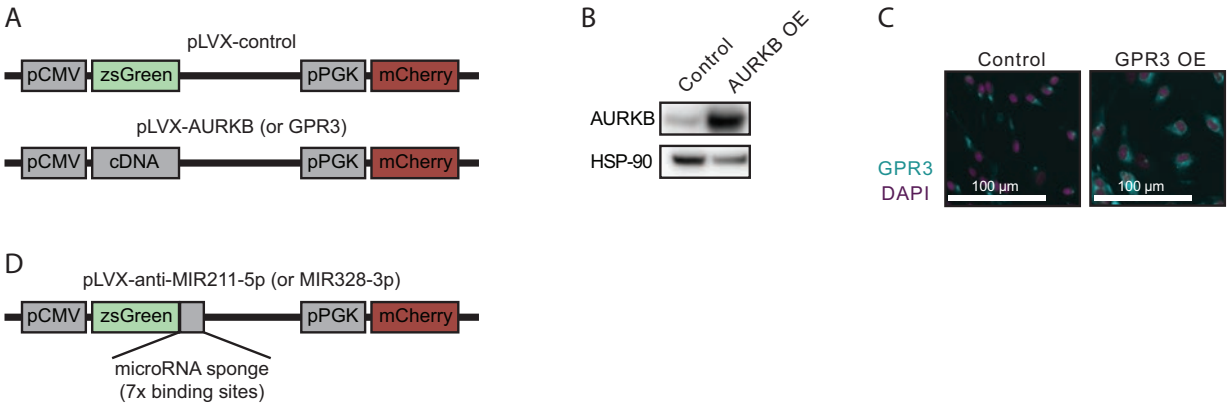

Supplemental Figure S2

Supplemental File 3 (related to Figure 2 and Figure 4)

(A) Design of pLVX vectors expressing either AURKB or GPR3. **(B)** Western Blot of AURKB expression in human melanocytes with or without lentiviral AURKB overexpression. HSP90 is the loading control. **(C)** Representative photomicrographs (20X) of immunofluorescence for GPR3 (green) or (Hoechst) (purple) in human melanocytes with GPR3 lentiviral overexpression (GPR3 OE) or without (Control) over-expression. **(D)** Design of pLVX vectors expressing microRNA sponges fused to zsGreen.

Supplemental Table S1 (related to Figure 1b)

Results of differential expression analyses performed on previously published databases of matched melanocytic nevi and melanoma-arising-from-nevi.

Supplemental Table S2 (related to Figure 1c)

Normalized read counts from small RNA sequencing performed on melanocytes derived from healthy human skin and melanocytic nevi.

Supplemental Table S3 (related to Figure 2)

Results of differential expression analyses performed on primary melanocytes nucleofected with microRNA or control mimics.

Supplemental Table S4 (related to Figure 2c)

Results from siRNA screen for EdU incorporation performed in primary melanocytes. Mean and standard deviation of triplicate screens shown for each gene. Column D indicates the microRNA predicted to targeted the gene.

Table S5 (related to Figure 4)

996 Results of differential expression analyses performed on primary melanocytes with or without $BRAF^{V600E}$
997 in +TPA or TPA-free conditions.